

Modification of the magnetic mineralogy in basalts due to fluid–rock interactions in a high-temperature geothermal system (Krafla, Iceland)

Belén Oliva-Urcia,^{1,2} Agnes Kontny,¹ Carsten Vahle³ and Anja M. Schleicher⁴

¹Institute of Applied Geosciences, Karlsruhe Institute of Technology, Hertzstrasse 16, 76187 Germany. E-mail: boliva@unizar.es

²Dpto. Ciencias de la Tierra, Universidad de Zaragoza, C/ Pedro Cerbuna 12, 50009 Zaragoza, Spain

³Eriksfiord AS, Kunnskapsparken, Postboks 8034, 4068 Stavanger, Norway

⁴Geological Sciences, University of Michigan, 1100 CC, Little Building, Ann Arbor, MI, USA

Accepted 2011 March 30. Received 2011 January 11; in original form 2010 May 10

SUMMARY

Active high-temperature (>150 °C) geothermal areas like the Krafla caldera, NE-Iceland, often show distinct magnetic lows in aeromagnetic anomaly maps suggesting a destruction of magnetic minerals by hydrothermal activity. The main alteration processes in such an environment are low-temperature oxidation (<350 °C, maghemitization) and fluid–rock interactions. We investigated the rock magnetic properties [natural remanent magnetization (NRM) magnetic susceptibility and their temperature and field variation] and the mineralogy, using X-ray diffraction, microscopic methods and electron microprobe analyses, of two drill cores (KH1 and KH3) from the rim of the Krafla caldera. The drill cores have distinctly lower NRM values (average <3 A m⁻¹) compared to younger surface basalts (average 20 A m⁻¹) along with a large variation in magnetic susceptibility (1.3 × 10⁻⁷ – 4.9 × 10⁻⁵ m³ kg⁻¹). The secondary mineral assemblage (sulphides, sphene, rutile and chlorite) indicates an alteration within the chlorite–smectite zone for both cores without depth zoning. Optical microscopy in combination with the Bitter technique and backscatter electron microscopy along with the thermomagnetic analyses allow distinguishing two different magnetomineralogical groups of titanomaghemite: (1) titanomaghemite with intermediate titanium concentration and probably high vacancy concentration, and (2) titanomaghemite with low titanium concentration and low vacancy concentration. The mineral assemblages, textures and magnetic properties deduced from the mentioned magnetic measurements indicate two-stage transformation mechanism: (1) Dissolution of titanium at low pH under oxidizing conditions. The ulvöspinel component of titanomagnetite and ilmenite forms rutile or sphene, and Fe²⁺ migrates out of the spinel lattice forming titanomaghemite. (2) Formation of pyrite and dissolution of remaining titanomaghemite under reducing and acidic conditions. The latter mechanism produces ghost textures (all titanomaghemite is transformed and only their former grain shapes are preserved), with only paramagnetic minerals left and ferrimagnetic minerals nearly dissolved. This mechanism could explain the significant magnetization loss, which is seen in many local magnetic anomaly lows within the oceanic crust and volcanic islands like Iceland or Hawaii. The production of nanoporous textures in titanomaghemites is suggested as a mechanism for the enhancement of the magnetic susceptibility values related to the hydrothermal alteration of Krafla.

Key words: Magnetic mineralogy and petrology; Rock and mineral magnetism; Hydrothermal systems.

1 INTRODUCTION

Magnetic properties are suggested to be sensitive indicators of hydrothermal alteration in basalts (e.g. Hall 1985) although complex alteration mechanisms are reported (e.g. Xu *et al.* 1997; Vahle *et al.*

2007). The reason for this complexity is the strikingly dynamic system (e.g. residence time of water in a hydrothermal system in Reykjanes, SW Iceland, is 5–6 yr; Kadko *et al.* 2007) under which the hydrothermal alteration process takes place over a long time period. In addition, the basalt can already show a large primary

variation of rock magnetic properties. Primary variations of remanence and susceptibility can be caused by different geochemical composition of the melt, which controls abundance (e.g. Vogt & Johnson 1973; Gee & Kent 1997) and chemical composition of the magnetic minerals (e.g. Marshall & Cox 1972). Additionally, cooling rate affects grain size and hence, the magnetic domain pattern (e.g. Kent & Gee 1994; Kontny *et al.* 2003). Other factors that influence remanence are the geomagnetic field intensity fluctuations (Gee *et al.* 1996; Juárez *et al.* 1998; Wang *et al.* 2005) and the viscous decay (Banerjee 1971).

The hydrothermal alteration processes depends on the fluid–rock interactions and redox conditions occurring at temperatures below 350 °C. In the Krafla area hydrothermal circulation started with the percolation of cold oxygenated meteoric water through NNE oriented rift-related fractures (Bödvarsson *et al.* 1984). Afterwards fluids are heated and enriched in volatiles from subsequent following fissure eruptions (Gudmundsson & Arnórsson 2002 and references therein). This evolutionary sequence might act repeatedly throughout the activity of the volcanic system. The chemical reactions between rocks and hydrothermal fluids are part of the fluid–rock interactions and can be monitored by the secondary mineral assemblages and water chemistry. Primary minerals of basalt and basaltic glass are unstable in contact with hydrothermal fluids. Glass is most easily altered, followed by olivine, pyroxene and plagioclase. According to dissolution experiments of Stefánsson *et al.* (2001) the following sequence of weathering preference is suggested in the Krafla area: Mg-olivine > Fe-olivine, Ti-rich magnetite > Ca-plagioclase, Mg-orthopyroxene > Fe-orthopyroxene, clinopyroxene > Na-plagioclase, F-apatite > Ti-rich ilmenite >> Ti-poor magnetite, Ti-poor haematite. These findings indicate that the stability of titanomagnetite is very sensitive to composition (higher content in Ti implies less stability under the same chemical-physical conditions). Apart from composition, grain size is an important factor that also influences the kinetic reactions (Pyzick & Sommer 1981; Poulton *et al.* 2004). The smaller the grains the faster the grains react. High-temperature oxidation and maghemitization diminish grain size due to the formation of ilmenite lamellae and the production of shrinkage cracks, respectively.

Oxidation of titanomagnetite at low temperature (<250–300 °C) producing titanomaghemite is a widespread process, which takes place preferably in water-dominated environments and is favoured under low pH conditions (Worm & Banerjee 1984). This process occurs when Fe²⁺ diffuses out of the structure of titanomagnetite/magnetite creating vacancies in the crystal lattice and producing a non-stoichiometric (Fe-deficient) metastable spinel polymorph of haematite (Prévot *et al.* 1968).

The effect of maghemitization on the magnetic properties of basalts has been broadly studied, but still it is not unequivocally understood and sometimes inconsistent. (1) Irving (1970), Marshall & Cox (1972) and Bleil & Petersen (1983) suggested the decrease of natural remanent magnetization (NRM) intensity. (2) Maghemitization seems to produce both, an increase in coercivity and a decrease in saturation magnetization in natural samples (e.g. Özdemir & O'Reilly 1982; Cui *et al.* 1994; Wang & Van der Voo 2004) but in synthetic samples also a decrease in coercivity is reported (Readman & O'Reilly 1972; Brown & O'Reilly 1999). (3) With respect to susceptibility, Cui *et al.* (1994), Wang *et al.* (2006) and Krása & Herrero-Bervera (2005) suggested a decrease of susceptibility with maghemitization, while others found no change for multidomain grains (Smith 1987), or even an increase (Özdemir & O'Reilly 1982; Brown & O'Reilly 1999). In addition, experimental work suggests that magnetic interactions increase bulk magnetic sus-

ceptibility (Gaillot *et al.* 2006), an effect that can take place in maghemitized samples due to the new formation of cracks and grain boundaries during the maghemitization process. (4) Curie temperatures increase (Ade-Hall *et al.* 1971) and cell parameter decrease with increasing oxidation parameter (z), which is the fraction of Fe²⁺ in the stoichiometric composition transformed to Fe³⁺. Some of these contradictions probably are related to different degrees of oxidation or inversion of titanomaghemite (e.g. Özdemir & O'Reilly 1982; Bleil & Petersen 1983; Özdemir 1987).

The aim of our study is to understand the processes that cause a significant low in the aeromagnetic map, the NRM decrease and the large magnetic susceptibility variation related to the hydrothermally altered basalts from the recently active geothermal system at Krafla, NE Iceland (Figs 1 and 2). We present a rock magnetic and microscopic characterization comprising the temperature dependence of magnetic susceptibility, thermal demagnetization of the natural magnetic remanence and field dependence of magnetic susceptibility measurements. Our data suggest that maghemitization is linked to fluid–rock interactions as the main mechanism for remanence loss and to the amplification of the range of the magnetic susceptibility values.

2 LOCATION OF KH1 AND KH3 DRILL CORES

The Krafla active geothermal system extends along a N–S oriented fissure swarm of 100 km length and 5–8 km width in the NE part of Iceland (Fig. 1a). The Krafla caldera, around 8–10 km in diameter, collapsed about 110 ka ago during the last interglacial period with the explosive eruption of rhyolitic and dacitic lavas (Saemundsson & Pringle 2003). The central volcano of 25 km in diameter evolves in less than 250 ka (Saemundsson 1978; Saemundsson & Pringle 2003). The age of the deepest part of the cores at Krafla (2 km) is considered to be less than 500 ka (Gudmundsson 1993). Postglacial volcanism in the Krafla area has been divided into two periods: the first one ended about 8 ka ago and the second, which is still active, started about 3 ka ago (Saemundsson 1991). Krafla was last active during 1975–1984 eruption episode (Krafla fires). The KH1 (200 m depth) and KH3 (400 m depth) drill holes are situated at the eastern rim of the caldera (Fig. 1b). The magnetic high in the area (53500 nT), which was measured during an aeromagnetic survey, corresponds to the Mt. Krafla, and the magnetic low (51000 nT) coincides with the caldera bottom where the Krafla geothermal field and fissure eruptions are situated (Leo Kristjánsson, personal communication, 2006). The same magnetic anomaly pattern occurs in Reykjanes Peninsula (SW Iceland), where the magnetic anomaly lows also coincide with the active geothermal fields (Gudmundsson *et al.* 1971; Dietze *et al.* 2011).

3 SAMPLE MATERIAL AND METHODS

The magnetic susceptibility of the full core (diameter 4.4 cm) was measured with a hand-held kappameter (KT-5, Geofyzica) at different depth intervals where material was available (Fig. 3). All together we made 1815 single measurements from about 210 m of KH1 and KH3 cores. The average distance between single measurements was 12 cm. The measurement sensitivity of the hand-held kappameter is 1×10^{-5} SI. Standard samples (2.5 cm in diameter and 2.1 cm in height) were selected with respect to the values of bulk susceptibility and lithology (some of these sample positions are shown in Fig. 3). The volume susceptibility (κ) was measured

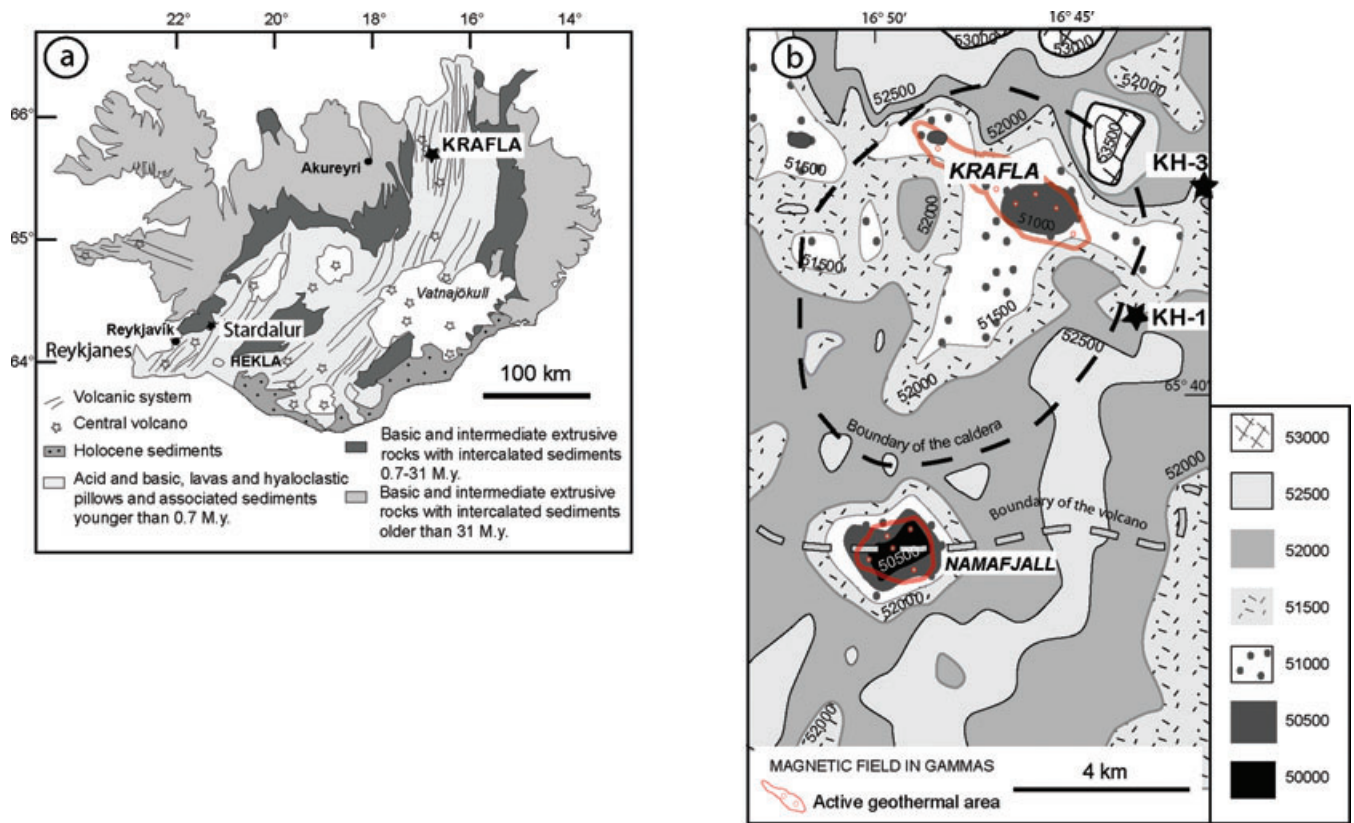


Figure 1. (a) Simplified geological map of Iceland. (b) Magnetic anomaly map with volcano and caldera boundary outlined in dashed lines (Gudmundsson *et al.* 1971), and the two drillholes KH1 and KH3. The dark grey areas with lower magnetic field correlate well with the active geothermal fields of Krafla and Namafjall. The numbers give the magnetic field in nT.

Table 1. Rock magnetic data for different basalt lithologies and andesite of KH1 and KH3 drill cores.

	Lithology	<i>N</i>	mass susceptibility ($10^{-5} \text{ m}^3 \text{ kg}^{-1}$) \pm <i>SD</i> (χ_{300})	NRM \pm <i>SD</i> (A m^{-1})	<i>Q</i> -ratio \pm <i>SD</i>
KH1	Basalt	9	2.29 ± 1.46	2.01 ± 1.39	0.802 ± 0.254
	Basaltic tuff	4	0.15 ± 0.124	0.61 ± 0.43	3.82 ± 3.06
	Vesicular basalt	7	1.13 ± 1.57	0.73 ± 0.72	1.67 ± 1.53
KH3	Basalt	47	1.2 ± 0.818	2.99 ± 2.88	2.73 ± 3.11
	Basalt breccia	4	0.264 ± 0.152	1.76 ± 1.02	5.59 ± 1.02
	Basaltic andesite	6	1.73 ± 0.291	5.65 ± 4.64	3.38 ± 3.26
	Pillow basalt	16	0.821 ± 0.626	3.76 ± 5.07	6.21 ± 9.81
	Porphyritic basalt	4	1.5 ± 0.551	3.29 ± 1.21	2.26 ± 0.24

Notes:

Mass susceptibility \pm *SD* is the mean susceptibility value normalized by mass and the standard deviation value.

N, number of analyses; NRM, natural remanent magnetization and its standard deviation;

Q-ratio, Koenigsberger ratio and its standard deviation.

again in the laboratory on these standard specimens using the KLF-3 susceptometer (Geofyzika now AGICO Inc.) at 30 and 300 A m^{-1} and 2000 Hz, and after weighting the samples, the mass normalized susceptibility was calculated (Tables 1 and A1). The hand-held kappameter measurements were compared with laboratory measurements on standard specimens. There is a linear relationship between both measurements (hand-held and KLF-3 at 30 A m^{-1}) with a high correlation coefficient ($R^2 = 0.888$, $n = 24$ for KH1; and $R^2 = 0.905$, $n = 82$ for KH3), although a general shift towards lower values for the hand-held kappameter measurements can be observed ($y = 0.435x + 1.532$ for KH1 and $y = 0.398x + 1.169$ for KH3), which can be explained by the small core diameter

of 4.4 cm compared to the diameter of the measurement coil of 6 cm. In spite of this deviation, hand-held kappameter measurements are useful to reveal the pattern of magnetic susceptibility versus lithology and depth, and are used in our study to select the sampling positions of standard specimens (Fig. 3). 60 samples were collected for rock magnetic laboratory measurements (see data in Tables 1 and A1) from the different lithological units. The standard samples were drilled from the lithological units of the drill cores from positions with low-, intermediate- and high-magnetic susceptibilities. From rock chips of the same sample we measured temperature dependence of magnetic susceptibility and subdivided the samples according to their behaviour into magnetically different groups.

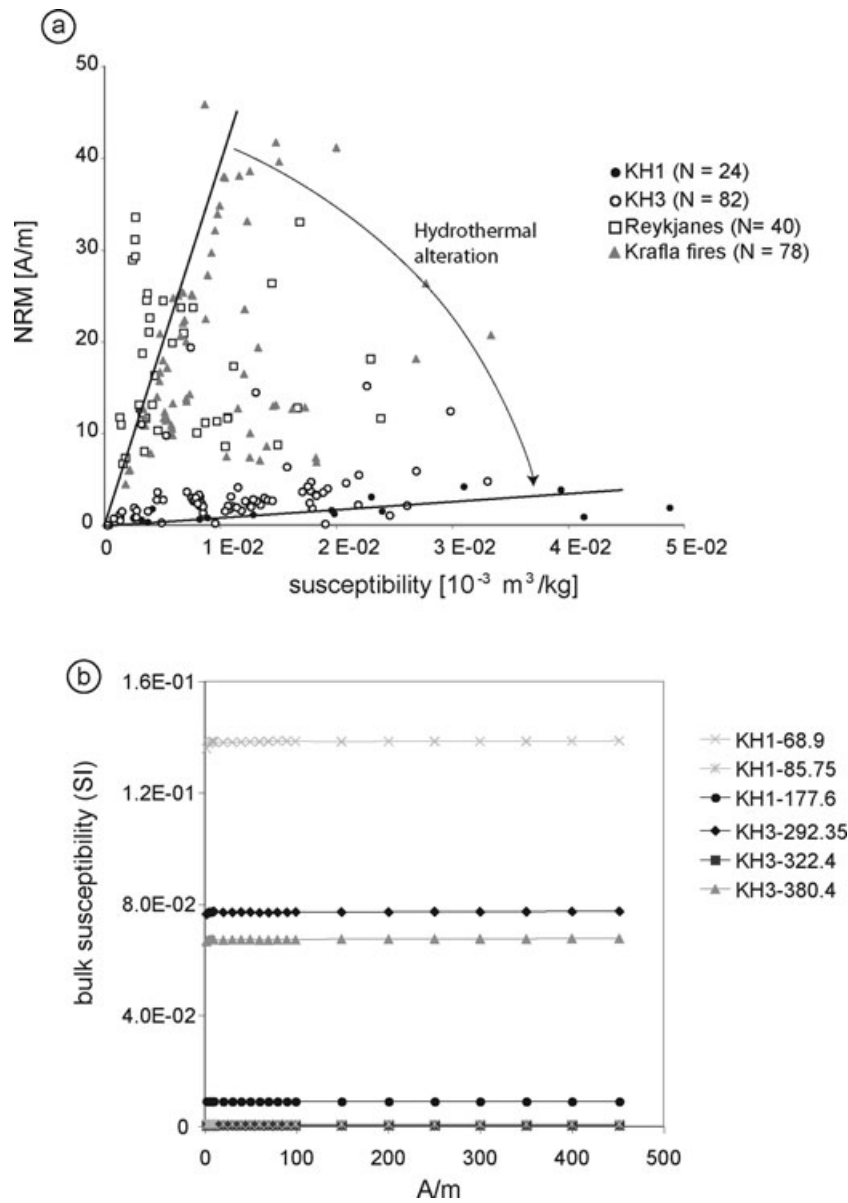


Figure 2. (a) NRM versus magnetic susceptibility of drill core samples KH1 and KH3 compared to basalts sampled from the surface at Krafla (Krafla fires) and Reykjanes (SW of Iceland). (b) Variation of the bulk magnetic susceptibility with respect to the applied magnetic field (in A m^{-1}) for the samples shown in Fig. 7 (note the little influence of the intensity of the applied magnetic field on the magnetic susceptibility values).

For representative samples of these magnetically different groups mineralogical investigations were carried out to identify the mineral composition and alteration assemblage, which accompanies the Fe-Ti oxides. The mineral assemblage of the bulk rock was determined using a Scintag θ - θ powder X-ray diffractometer with an accelerating voltage of 40 kV, a filament current of 35 mA and a $\text{CuK}\alpha$ radiation source at the University of Michigan, USA. A total of 11 samples from different depths were selected for X-ray diffraction (XRD) analyses. The preparation of the rock samples followed the analytical methods described by Moore & Reynolds (1997). Randomly oriented powder samples, as well as oriented textured samples (air-dried and ethylene glycolated) were prepared to identify the individual bulk mineralogy and the clay mineralogy. Treatment with ethylene glycol causes interlayer expansion of smectite swelling layers (shifting reflections towards higher d -values) and allows recognition of discrete smectite and

mixed layered C-S (chlorite and smectite type layers) phases. Measurements of peak heights, peak areas and peak widths of tracings were made using the MacDiff software (<http://www.geol-pal.uni-frankfurt.de/Staff/Homepages/Petschick/Classicsoftware.html>).

Oxide textures were characterized using reflected light microscopy with a cover of ferrofluid, and scanning electron microscopy (SEM) in backscatter mode (LEO 1530, from LEO company). 12 thin sections from KH1 and 13 thin sections from KH3 were studied. Samples were selected according to the magnetic groups to examine the texture and mineralogical content of samples with different lithology and susceptibility values. The application of ferrofluid (Bitter 1931; for an application in basalts see also Kletetschka & Kontny 2005) allows a separation of ferri-magnetic minerals, because the ferrofluid sticks only to magnetic phases with a large magnetic gradient produced by grains with large demagnetization fields such as titanomagnetite/magnetite,

at acceleration voltage of 15 kV with the NORAN System Six from Thermo Electron Corporation. Electron microprobe analyses using a CAMECA SX50 were done for three selected samples at the KIT.

For the temperature dependence (-194 to 15 °C and from room temperature to 700 °C) of magnetic susceptibility (κ - T) a KLY-4S kappabridge (working at 300 A m^{-1} and 875 Hz) combined with a CS-L/CS-3 apparatus (AGICO Inc.) was used. Heating/cooling rates range between 3 – 4 and 11 – 14 ° min^{-1} for the low-temperature and high-temperature run, respectively. The high temperature runs were done in an argon atmosphere to avoid mineral reactions with oxygen during heating (flow rate of 110 ml min^{-1}). Some samples were also measured in an air-flow of the same rate. The raw data were corrected for the empty cryostat/furnace and normalized. In this work the transition at low temperatures and the Néel or Curie temperature (T_N or T_C) were determined graphically using the peak temperature as described in Lattard *et al.* (2006) and/or the inverse susceptibility method (Petrovsky & Kapicka 2006) when transitions between ferromagnetic s.l. and paramagnetic behaviour were gradual. A total of 12 samples from KH1 and 22 samples from KH3 were analysed. The samples were selected depending on the magnetic susceptibility value (high and low) for the different lithological units in the cores.

Measurements of remanent magnetization of 53 samples were done with a JR5A spinner magnetometer (AGICO Inc.). For stability tests, alternating field (AF) demagnetization was performed in 21 samples in peak fields up to 160 mT with a MI AFD 1.1 from Magnon International. Stepwise thermal demagnetization up to 700 °C was done in 20 samples with the Thermal Demagnetizer MMTD1 (Magnetic Measurements).

4 ROCK MAGNETIC PROPERTIES

Magnetic susceptibility measurements along the drill core for different depth intervals of KH1 (altered tholeiitic basalt, tuff and hyaloclastite) and KH3 (lava flows of altered tholeiitic basalt, breccias, tuffs and pillow basalts) are shown in Fig. 3. The lowest values of susceptibility are in the higher porous materials such as hyaloclastites, tuffs and in the vesicular basalts ($<2 \times 10^{-7}$ m³ kg⁻¹ in KH1 and $<3 \times 10^{-7}$ m³ kg⁻¹ in KH3), whereas the fine-grained andesite, basalts and basalt intrusions show the highest susceptibility values (4.9×10^{-5} m³ kg⁻¹ in KH1 and 3.3×10^{-5} m³ kg⁻¹ in KH3).

Tables 1 and A1 show the magnetic parameters measured and calculated from the standard cylindrical samples. The discrimination diagram in Fig. 2(a) displays a wide range of susceptibility values (1.3×10^{-7} to 4.9×10^{-5} m³ kg⁻¹), whereas NRM values are rarely higher than 5 A m^{-1} (only six out of 106 samples have NRM > 20 A m^{-1}). In fresh surface basalts younger than 11 ka, higher NRM values (up to 46 A m^{-1} with a mean value of 20 A m^{-1} for $N = 78$) and lower susceptibility values (below 3.34×10^{-5} m³ kg⁻¹ with a mean value of 9.05×10^{-6} m³ kg⁻¹) compared to the drill core data were observed. The trend from high NRM and intermediate susceptibility values in fresh basalt towards low NRM and a strong variation in susceptibility values in altered basalts seems to be related to the hydrothermal alteration of the samples.

The median demagnetizing field (MDF) determined from AF demagnetization of NRM has an average of 19 mT for KH1 and 23 mT for KH3 indicating moderate coercivity values (Table A1). The Königsberger ratio (Q ratio), which is the ratio between the remanent and the induced magnetization, is very low in both drill

cores (average 1.6 in KH1 and 3.4 in KH3) compared to the young surface basalts (average of Q ratio: 27) indicating only a weak dominance of remanent over induced magnetization. The field dependence of magnetic susceptibility (f_{Hd}), which can be used as a first indicator of Ti content in titanomagnetite (see e.g. de Wall 2000), has low values in both KH1 and KH3 drill cores except for few samples (Fig. 2b and Table A1) indicating at first sight, a low Ti-concentration in titanomagnetite. Even if we measure magnetic susceptibility at 21 different applied fields, no significant change was found for most of our samples (Fig. 2b). This behaviour normally indicates a very low Ti concentration in the titanomagnetite (e.g. Jackson *et al.* 1998). The field dependence of magnetic susceptibility in titanomagnetite, however, can be masked by different compositions occurring in the same sample, small grain sizes or textural effects (e.g. Vahle & Kontny 2005).

5 MINERALOGICAL RESULTS

5.1 XRD analysis

Oriented textured X-ray diffraction analysis indicates pyroxene (augite and/or diopside), chlorite, chlorite–smectite (C–S, corrensite and/or vermiculite) and feldspar (plagioclase and minor K-feldspar) minerals in all samples investigated. Calcite, quartz, zeolites (mainly heulandite), pyrite and illite–smectite are present in some samples. The weak 002 chlorite peak at ~ 7 Å in core KH1 shows the occurrence of a Mg-rich C–S (vermiculite) mineral (Moore & Reynolds 1997), whereas a first order peak at 29.5 Å shows the additional occurrence of a well-ordered C–S (corrensite) at 174.7 m. In core KH3, vermiculite does not dominate based on the strong 002 chlorite peaks at ~ 7 Å. However, first-order peaks at 29.5 Å show the occurrence of corrensite minerals, with an additional C–S phase at 49.3 m depth based on a slight peak shift. The presence of zeolites is irregular with depth, with the highest amount of heulandite at KH1– 83.2 . The mineral assemblage indicates a facies equivalent to the chlorite zone with no depth variation for both cores since chlorite seems to be present in all samples. The occurrence of C–S and zeolites indicates a retrograde alteration into the zeolite facies, which may have affected KH1 more than KH3 based on the amount of C–S and heulandite.

5.2 Petrography

The main rock forming minerals are silicates, as described by the XRD data. Plagioclase phenocrysts occur in prismatic shapes with a range of grain sizes varying from 100 to 300 μm (exceptionally up to 3 mm) and laths of 20 – 100 μm were observed in the matrix (Fig. 4a). Pyroxenes identified in polarized light were altered to chlorite or other phyllosilicates. Vesicles and voids are filled with chlorite, quartz and calcite (Figs 4a and b). Chlorite is the most characteristic secondary mineral in KH3 at all depths. The total abundance of ferrimagnetic minerals (titanomagnetite) was estimated from thin-section observations to be about 5 – 10 vol. per cent. Sulphides (mainly pyrite and chalcopyrite), rutile, sphene and ilmenohaematite were also identified. Our findings agree with previous work on opaque minerals in Krafla drill core No. 7 (Steinthórsson & Sveinbjörnsdóttir 1981), although in our study no goethite occurs.

Titanomagnetite (tmt, in this paper used as a generic term for titanomagnetite, mt for magnetite, tmgh for titanomaghemite and mgh for maghemite) forms cruciform, skeletal and euhedral grains of <2 up to 150 μm in size. Sphene is very abundant and has

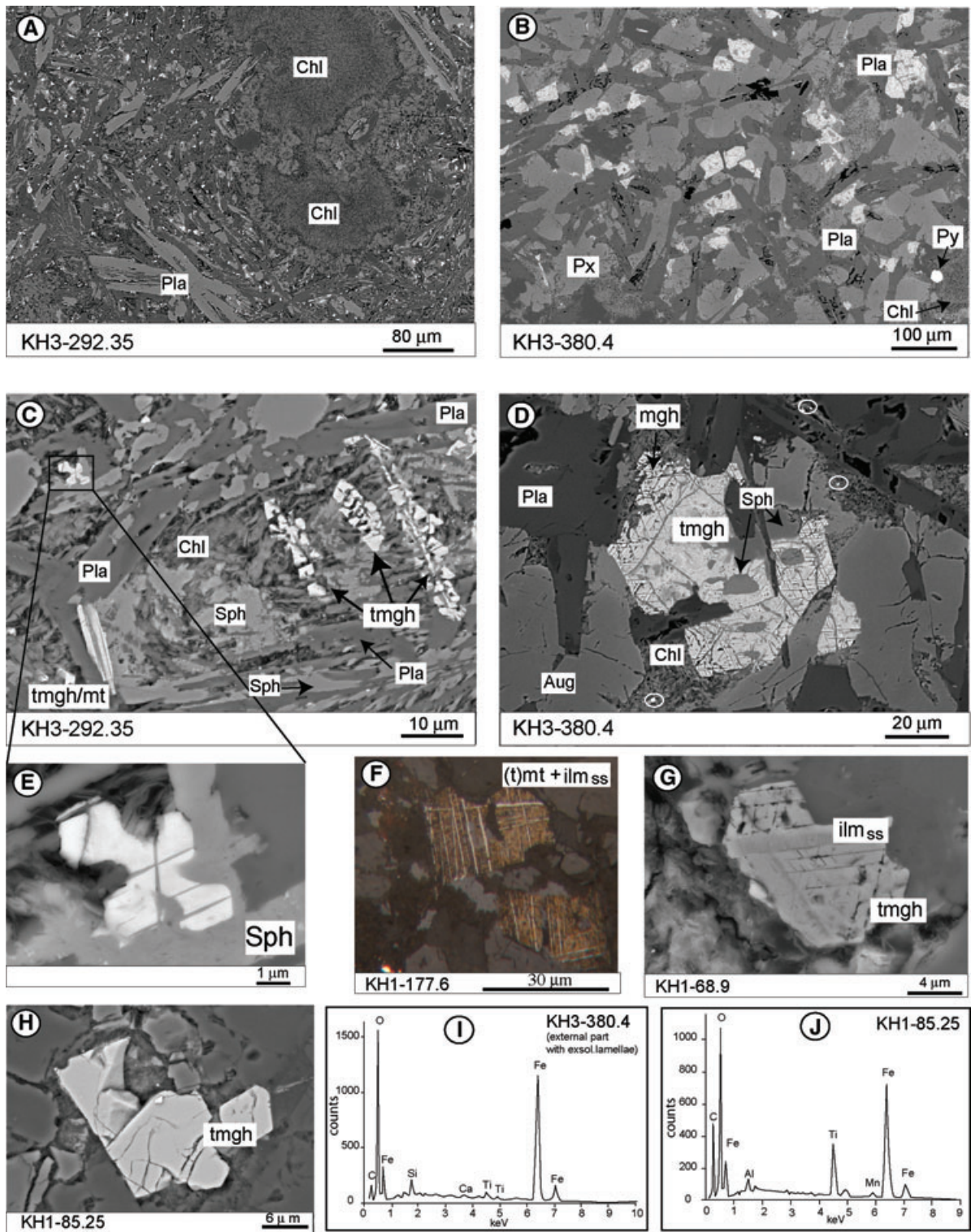


Figure 4. Electron microscopy images in backscatter mode. (a) and (b) show, respectively, fine- and coarse-grained basalt texture and voids filled with chlorite. (c) and (d) are enlargements of (a) and (b), showing fine- and coarse-grained titanomaghemite (tmgh) and sphene. In (d), exsolution lamellae in the outer part of the grain, shrinkage cracks filled with sphene (Sph) and transformation of tmgh to sphene in the inner part of the grain are shown (grey patches in d). Pyrite (Py) grows within chlorite (very small grains with white circles). (e) Cruciform grain enlarged from (c). (f) Large and (g) small grains of tmt/tmgh with different thick lamellae of ilmenohaematite solid solutions (ilm_{ss}). (f is an optical microscope image under reflected light, coated with ferrofluid and in oil immersion). (h) Shrinkage cracks in homogeneous tmgh (KH1-85.25). (i), (j) EDX analysis from grains shown in (d) and (h), respectively. Pla, plagioclase; Chl, chlorite; clays; Px, pyroxene (augite, Aug); Sph, Sphene.

been observed as alteration product of ilm_{ss} and tmt (Figs 4c and d). Ilmenohaematite (ilm_{ss}) occurs as exsolved lamellae within tmt (Figs 4f and g) and as skeletal, subhedral grains of <1 to 100 μm in size. Sulphides, mostly pyrite (Fig. 4b), but sometimes chalcopyrite, and sphalerite appear. In general, the sulphide grains are subhedral, up to 200 μm in size and in some samples a thin seam around sulphides of secondary minerals such as quartz occurs. In some samples the sulphides concentrate near the border of vesicles indicating the last precipitation from hydrothermal fluids.

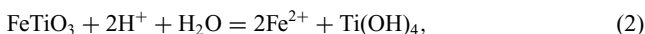
The textures of the ferrimagnetic Fe-Ti oxides indicate both, quick cooling with small cruciform and skeletal shapes (Figs 4a, c and e) and slow cooling with large, euhedral Fe-Ti oxide grains (Figs 4b and d). Exsolution lamellae occur in both cores at different depths (Figs 4f and g). They form during high-temperature oxy-exsolution at about 600 °C (Haggerty 1991) after crystallization of the lava, typically under subaerial conditions or during slow cooling in dyke intrusions or massive lava flows. High-temperature oxidation produces a Ti-poor titanomagnetite. Some samples also show thick ilm_{ss} lamellae related to a primary origin and not to high-temperature oxy-exsolution (Fig. 4g).

Further oxidation and mineral reactions took place at lower temperatures (250–350 °C) as part of the fluid–rock interactions. Low-temperature oxidation with diffusion of Fe²⁺ out of the titanomagnetite/magnetite crystal lattice will produce a cation-deficient tmt/mt and tmgh/mgh as end product. With diffusion of iron, the lattice parameters become smaller and eventually, the oxidized grain will crack (Petersen & Vali 1987). In the Krafla drill cores all samples show some degree of maghemitization with shrinkage cracks as typical feature independent if they already suffered a high-temperature oxy-exsolution (Figs 4d and i) or not (Figs 4h and j). The next section will explain the observed alteration features in relation to fluid–rock reactions.

5.3 Hydrothermal alteration of Fe-Ti oxides

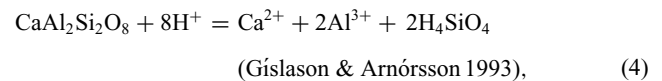
In the Krafla drill cores, secondary minerals like iron-sulphides, sphene, chlorite and quartz are commonly associated with tmgh (Figs 4d and e and 5a and b). Dissolution of ferrimagnetic grain rims is ubiquitous, especially where they are in contact with chlorite (Fig. 5b). The most altered samples show ‘ghost textures’: SEM investigations revealed for these textures Ti-oxide lenses as reaction products of the tmgh/ilm_{ss} grains. The Ti-oxide lenses are oriented parallel to the former ilm_{ss} lamellae (Fig. 5c). Other strongly altered samples show sphene (enriched in Mn) and subidiomorphic sulphide grains as products of titanomagnetite dissolution. In Fig. 5(d) sphene mimics the former high-temperature oxidation ilm_{ss} lamellae, while the tmt host is dissolved. Only the former grain shapes are preserved. This extreme alteration (ghost texture) is more abundant in KH1.

These mineral textures imply strong fluid–rock interactions, which allow the movement of elements. The end product of rutile in some of the ‘ghost texture’ samples shows that Ti can originate from the dissolution of Fe-Ti oxides, for example, from the ulvöspinel component, which is undersaturated in geothermal waters (Stefánsson 2001) or ilmenite.



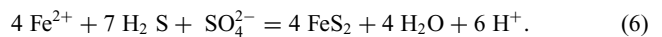
Reactions 1 (ulvöspinel) and 2 (ilmenite) are examples of dissolution of Fe-Ti oxides at a low pH and in oxidized environment (Stefánsson 2001). They indicate the mobility of Ti in the aqueous systems with rutile as a final product (reaction 3). Furthermore, these reactions imply a connection to the oxidation mechanism during maghemitization of tmt, which is defined by diffusion of Fe²⁺ to the surface of the crystal, leaving the tmt spinel structure unchanged but part of the octahedral sites vacant. The intimate intergrowth of tmgh with sphene and cation-deficient mt (mgh; Fig. 4d), can then easily be explained by the relation between oxidation and mineral reaction.

Not only rutile but also sphene forms ubiquitous as secondary mineral and replaces the ferromagnetic minerals in the Krafla drill cores (Figs 4 and 5). It is especially abundant in samples where no ferrimagnetic minerals are seen. The dissolution reaction of Fe-Ti oxides, which produces sphene (CaTiSiO₅), can be represented as a reaction where the required calcium and silica are provided from the dissolution of pyroxene or plagioclase.

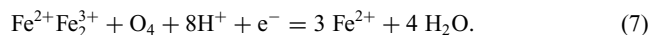


The Fe²⁺, which is released to the fluid from reaction 1 or 2 as well as from the dissolution of pyroxene can then be used to form chlorite, which is the most ubiquitous secondary mineral in the KH1 and KH3 drill cores.

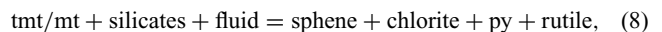
Temperature, pH and redox potential play important roles in these reactions. The activity of Fe²⁺ strongly decreases with increasing temperature since the redox potential decreases with increasing temperature (Gudmundsson & Arnórsson 2002; Stefánsson & Arnórsson 2002 and reference therein). Sulphides (mainly pyrite) occur as newly formed grains next to relicts of the magnetic Fe-Ti oxides and are very abundant in ‘ghost texture’ samples (Fig. 5d). Pyrite can be formed according to the reaction described by Ármannsson *et al.* (1989).



The production of Fe-sulphides increase the quantity of protons H⁺ in the fluid, thus the pH will decrease, which can lead to further alteration of mt as described in White *et al.* (1994):



This reaction sequence explains why in samples with high sulphide content the magnetic Fe oxide is dissolved (‘ghost texture’) and they also explain our microscopic observations according which the titanomaghemite transforms into sphene and/or rutile. Additionally to sphene and rutile, chlorite and clay minerals as well as Fe-sulphides belong to the alteration assemblage. We can summarize our microscopic observations with



which indicate that tmt/mt suffered extensive fluid–rock alteration until the grains become totally dissolved. All samples in Krafla show some degree of maghemitization (low-temperature oxidation) hence, the ferrimagnetic grains in Krafla samples are cation-vacancy titanomagnetite: titanomaghemite or maghemite (tmgh/mgh).

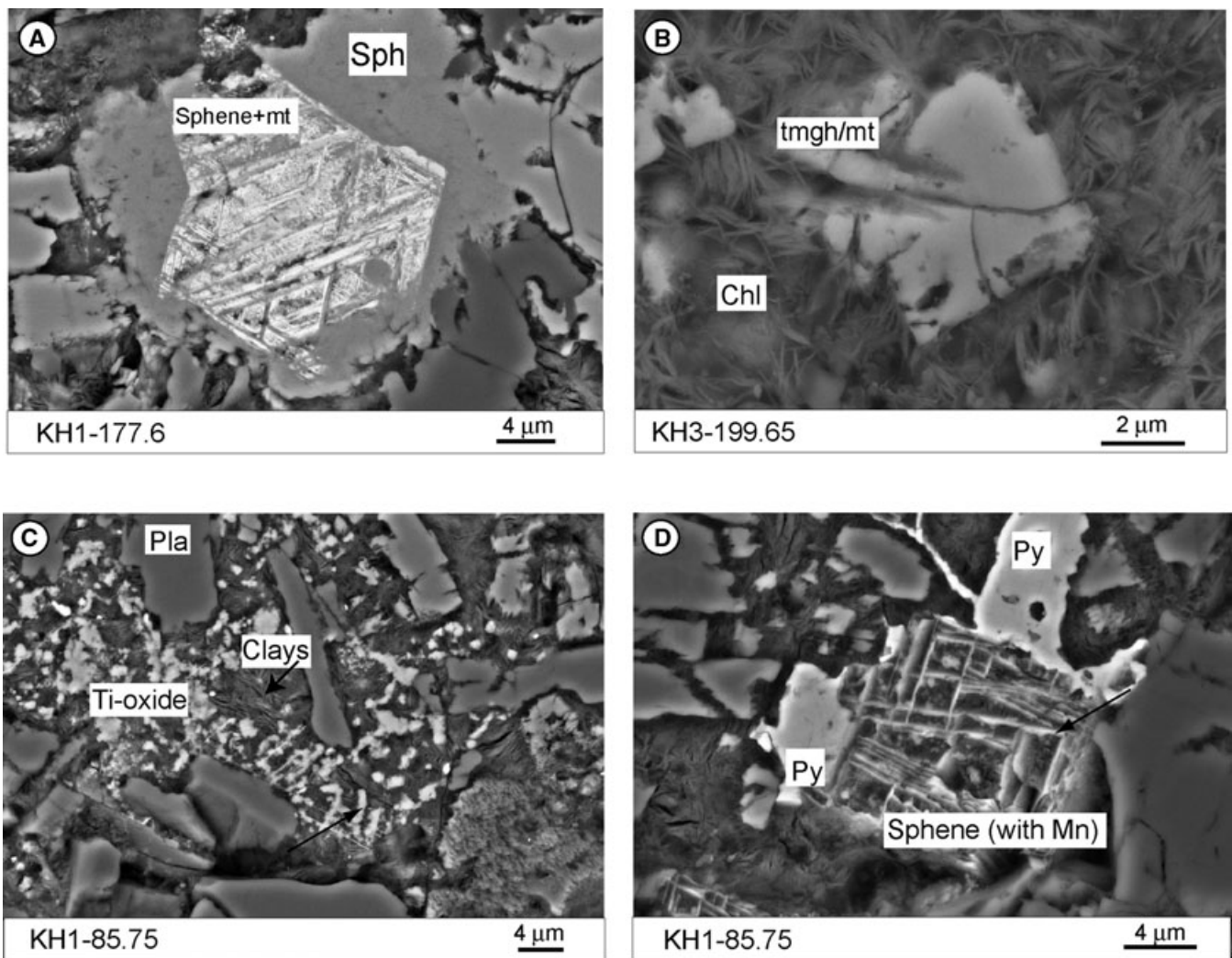


Figure 5. BSE images of oxide textures. (a), (b) show intermediate grades of alteration: (a) altered cation deficient mt surrounded by sphene (Sph); (b) dissolved tmgh/mt surrounded by chlorite. (c), (d) High grades of alteration ('ghost textures'): (c) Relicts of ilm_{ss} lamellae transformed to Ti-oxide (arrow). (d) Relicts of ilm_{ss} lamellae transformed into sphene (arrow) rich in Mn, with pyrite grown next to the former tmgh.

5.4 TEM investigations

To better understand the titanomagnetite to maghemite transformation, TEM was done. An unusual nanoporous microstructure in titanomaghemite of the two investigated samples KH3-292.35 (fine grained, Figs 4a, c and e) and KH3-380.4 (coarse grained, Figs 4b and d) was observed. Such a structure is a strong indication for areas with vacancies, which break off due to ion bombardment during TEM analyses (see inset in Fig. 6a). This texture is distinctly different compared to fresh tmt from surface basalt samples of Reykjanes (Fig. 6b). The fresh tmt grains show a homogeneous appearance of dendritic crystals, a face-centred cubic lattice and some Ti in the structure [from T_C , a tmt composition of $X_{Usp} = 0.55$ is calculated according to the equation given in Lattard *et al.* (2006) for synthetic tmt], as it is typical for fresh, primary tmt (e.g. Zhou *et al.* 1999). In the altered Krafla drill core sample (Fig. 6a), the selected area electron diffraction (SAED) pattern indicates face-centred cubic lattices, sometimes with ordered superstructure reflections and in few cases a tetragonal superlattice. This observation is in accordance to earlier descriptions (Xu *et al.* 1997 and references therein), where three symmetries have been proposed for maghemite, one corresponding to a face-centred cubic structure, one to a tetragonal

superlattice and one to a primitive cubic superlattice. EDX analyses show that both Fe and O are present but no Ti. Small peaks between 5 and 6 KeV in Fig. 6(a) indicate some Cr. In this TEM study we only observed maghemite grains without Ti.

6 THERMOMAGNETIC RESULTS

6.1 Temperature-dependent magnetic susceptibility between -194 and 700 °C

Curie temperature defines the transition temperature from magnetic ordering (such as ferro- or ferrimagnetism) to paramagnetism whereby the directions of the magnetic moments are randomly oriented in the latter stage. The Curie temperatures (T_C) determined from κ - T curves are very sensitive to Fe-Ti oxide composition (e.g. Lattard *et al.* 2006 and references therein). Additionally to T_C determination, κ - T curves are very sensitive to mineral reactions, which occur during the heating if magnetic phases become unstable. The stability of the original magnetic phases can be monitored by the degree of reversibility of the heating and cooling runs in air and in argon atmosphere (e.g. Deng *et al.* 2001; Vahle *et al.* 2007). κ - T

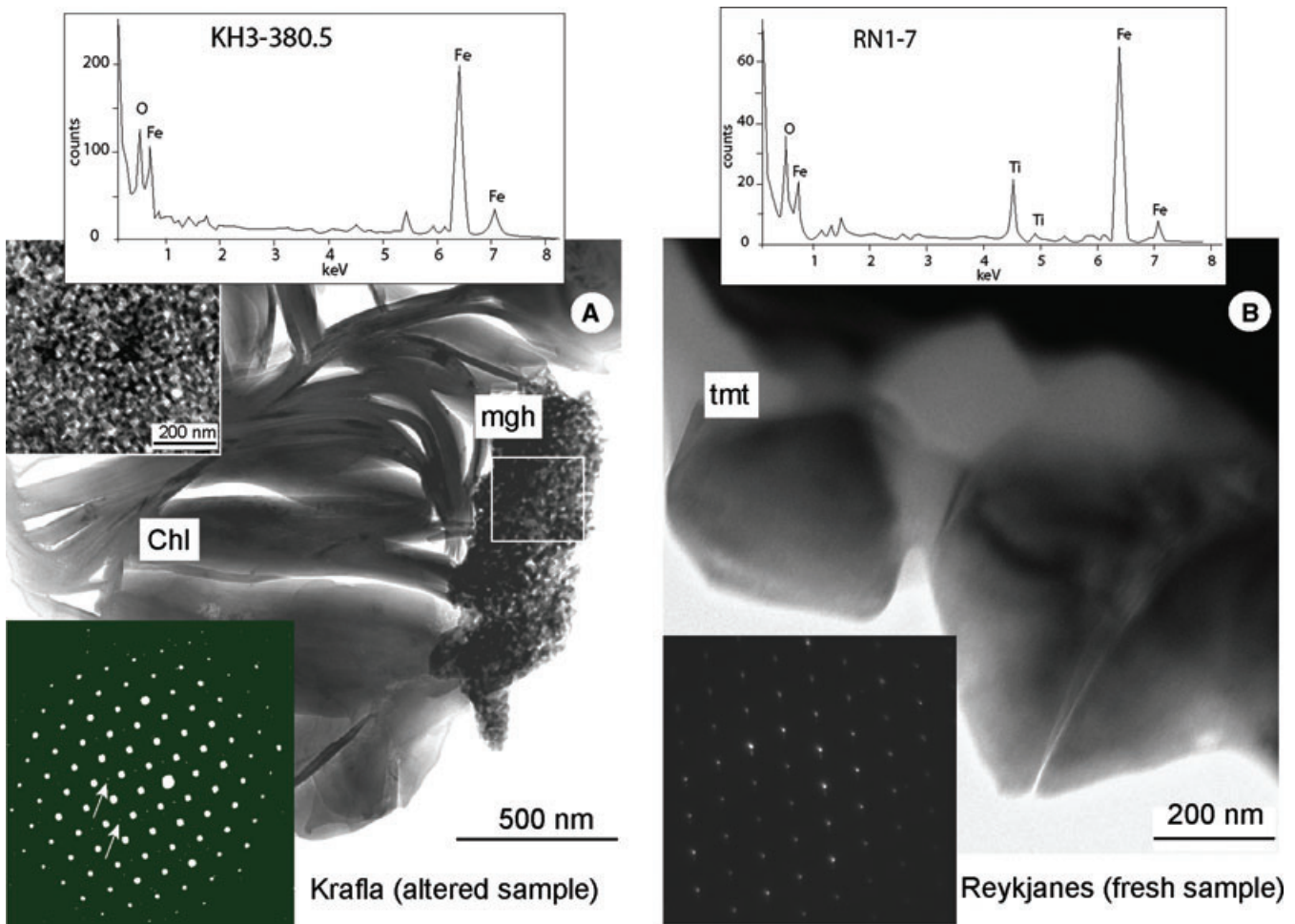


Figure 6. TEM bright field images, diffraction patterns and qualitative chemical composition from (a) Krafla sample of type II (hydrothermally altered) and (b) Reykjanes sample (fresh sample). Selected area electron diffraction (SAED) at Krafla shows superstructure reflections (marked with an arrow) in a face-centred structure. In Reykjanes no superstructure reflections are observed in the face-centred cell.

curves from surface samples of Krafla are reversible (comparable with κ - T curves from synthetic tmt shown in Lattard *et al.* 2006), which indicates very little (if any) metastable magnetic Fe-Ti oxides. In contrast, all samples but one from the Krafla drill cores show non-reversible κ - T curves, interpreted to indicate different degrees of maghemitization, which is in agreement with the ubiquitous occurrence of shrinkage cracks seen microscopically and the unusual nanoporous microstructure seen in Fig. 6(a) in the TEM.

From the κ - T curves we distinguished three main types: II, I-II and III (Fig. 7). The roman numbers indicate that these types show irreversible κ - T curves and they are interpreted as low-temperature oxidized varieties of the types named by Arabic numbers in Kontny *et al.* (2003, see fig. 4 therein), which refer to stable magnetic phases during κ - T measurements. In general, type I/I means, that T_{CS} are below 400 °C (indicating intermediate Ti composition in titanomagnetite/titanomaghemite), and after observing the samples under the optical microscope, it is seen that the grains are more or less homogeneous. Type 2/II show T_{CS} in the range from about 480 to 585 °C indicating near end-member magnetite compositions of titanomagnetite/titanomaghemite with or without a Verwey transition (T_V) near -152 °C (transition from cubic to monoclinic symmetry in magnetite during cooling). This type mostly occurs in samples with high-temperature oxy-exsolutions.

Type II in the Krafla samples occurs in all lithologies except for the tuff layers of KH1 and only in basalts from KH3 (Figs 2, 7a and b and 8a). While in KH1 only a few samples show a decay in susceptibility near the T_V during κ - T measurement between -194 and 15 °C (Fig. 7a), the KH3 samples show a distinct T_V between -144 and -163 °C (Fig. 7b). T_{CS} in the heating run range between 534 and 582 °C in KH1, and between 568 and 587 °C in KH3. Mostly two decays in susceptibility were observed for these samples suggesting the presence of two phases: Ti-poor mgh (not reversible part) and minor mt (second decay in the heating run and presence of T_V), whereas in the $1/\kappa$ curve (Petrovsky & Kapicka 2006) two inflection points are found (Table A2). The susceptibility in the cooling run is always lower than in the heating run and it shows two different phases (Figs 7a and b and 8a).

Second runs at low temperature either show the T_V at even lower temperatures (< -152 °C) or do not show the T_V at all. However, a second heating-cooling run of samples KH3-380.4 and KH1-85.25 (Figs 7b and 8a in grey) is reversible with the first cooling curve. This behaviour strongly suggests that during the first heating in argon atmosphere, a stable tmt composition has been created indicating that a reaction took place during the argon atmosphere experiments, producing a close-to-stoichiometry titanomagnetite. This κ - T behaviour is independent of texture type (Figs 4d and h).

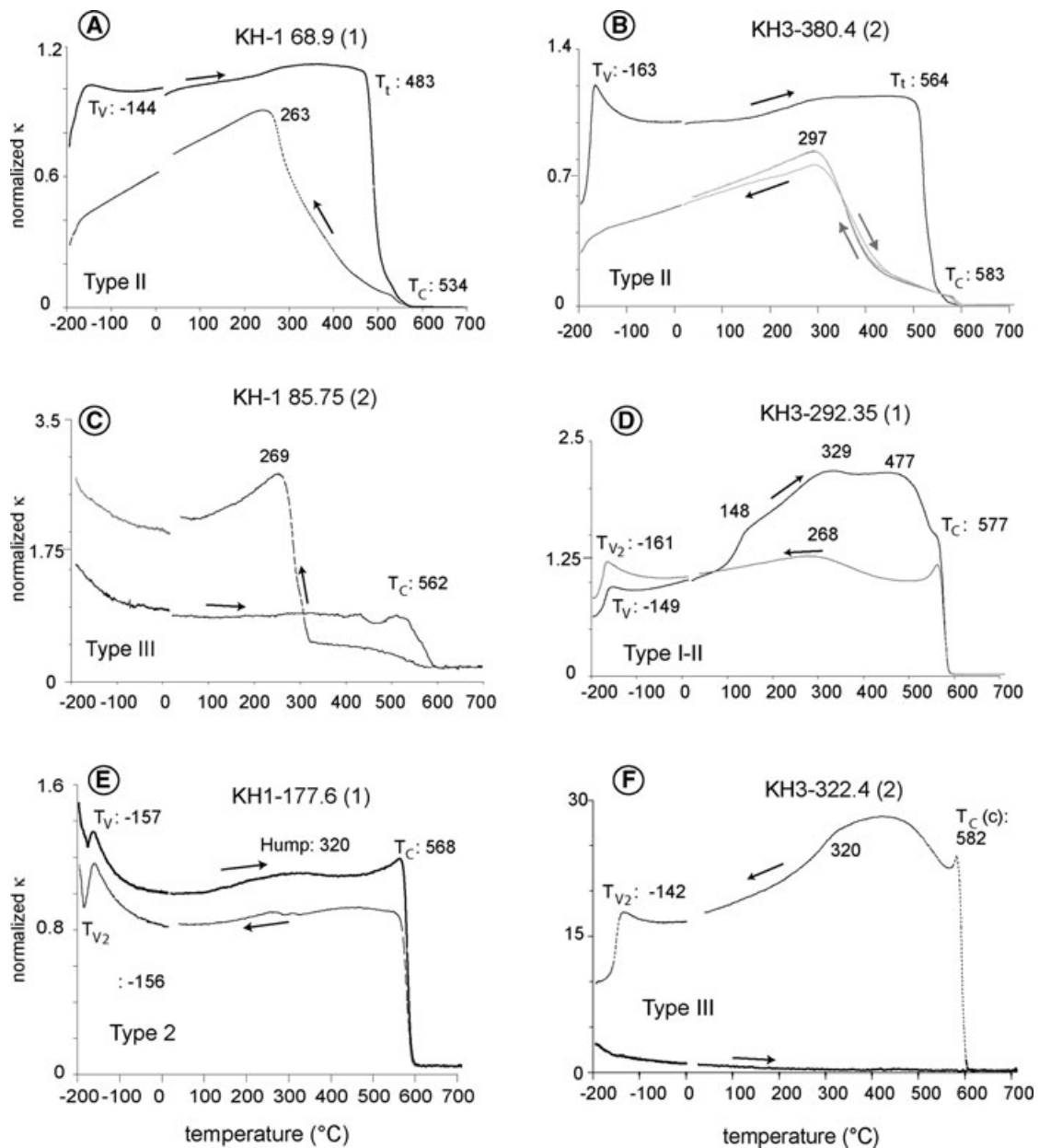


Figure 7. κ - T curves with T_V , T (intermediate inflection points, not differentiated) and T_C marked in degree Celsius (see Table A2). Note that type II in KH3 shows a second heating and cooling run with grey arrows. Type II curves have reversible runs after the first heating-cooling run. See text for further explanations.

Type I-II is only present in KH3 (Fig. 7d). These curves show a T_V between -144 and -161 °C and a reversible high-temperature phase (T_C between 561 and 633 °C), which indicates that magnetite/maghemite close to stoichiometry is present (as in type II). The second low temperature run usually shows no T_V or the T_V shifts to lower temperatures (see Table A2) indicating that this magnetite/maghemite is cation-deficient or impure. The increase in susceptibility with several humps, for example, at 148 , 329 and 477 °C in the first heating run (Fig. 7d) suggests that mt/tmgh occurs together with unstable intermediate phases with different Ti concentration. Although these phases are ferromagnetic during heating, they seem to vanish after heating to 700 °C. In the cooling curve, the pure magnetite is recovered but the intermediate Ti-bearing ferromagnetic phases are nearly destroyed and only a faint hump at 268 °C survived.

Type III curves show no T_V and a decrease of susceptibility, which is typical for paramagnetic behaviour (Figs 7c and f). The cooling curve displays a strong irreversible behaviour with much higher susceptibility compared to the heating run and therefore is distinctly different to the other types. A strong increase in susceptibility occurs below 300 °C in the cooling run of three samples in KH1 indicating the new formation of a ferromagnetic phase (Fig. 7c). We suggest that this new ferromagnetic phase is pyrrhotite, which has formed during the heating in an argon atmosphere from pyrite, which is abundant in this type of samples. Similar observations are described, for example, in Just (2005). Repeated heating (not shown) confirms a T_C at 310 °C, which is typical of pyrrhotite. In sample KH3-322.45 there is formation of magnetite and Ti-maghemite instead of pyrrhotite (Fig. 7f). All these samples contain secondary sulphides, but in different amounts as seen by optical and electron

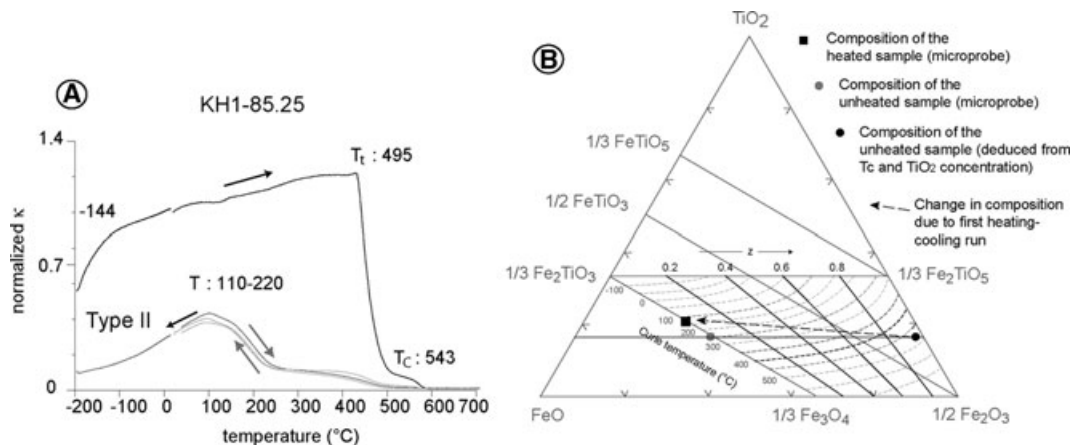


Figure 8. (a) κ - T curve for sample KH1-85.25 with first (black arrows) and second (grey arrows) heating-cooling cycles. (b) Ternary diagram FeO-TiO₂-1/2Fe₂O₃ with mineral chemical data of sample KH1-85.25 measured before and after heating (see Table 2). Lines with z (oxidation degree) and Curie temperatures for maghemites are from Readman & O'Reilly (1972) using the software Plot1.1.1 by John (2004). See text for further explanations.

microscopy. Our observations suggest that type III shows the highest degree of hydrothermal alteration causing the strongest decay of NRM and magnetic susceptibility.

Only one sample shows a type 2 behaviour (KH1-177.6; Fig. 7e) with a good reversibility between heating and cooling run and a sharp decay at 568 °C, indicating a near magnetite composition in κ - T curves. Only a faint hump at around 300 °C in the heating run seems to be not reversible. The Verwey transition occurs at -157 °C and a second low-temperature measurement confirms this T_V , indicating stable behaviour during heating. Such κ - T curves are typical for high-temperature oxidation of titanomagnetite (e.g. Kontny *et al.* 2003).

6.2 Transformation of metastable titanomaghemite into stable titanomagnetite during κ - T measurement

During repeated κ - T measurements in argon atmosphere we observed the formation of stable magnetic phases from unstable ones. Therefore we have done electron microprobe analyses of the ferromagnetic Fe-Ti oxide before and after heating (Table 2). For this experiment we chose a sample with type II behaviour and a relatively low transition temperature of 495 °C (and a T_C of 543 °C), indicating the presence of two phases, one phase with significant amount of Ti in the titanomaghemite and another magnetic phase with lower Ti content before heating. A compositional gradient between core and rim of the studied grains was not found. The analysed tmgh grains are about 20 μ m in size and dissected by shrinkage cracks, which widen after heating. The electron microprobe analyses (about four analyses per grain) clearly confirm a change in composition from the unheated to the heated sample (Table 2, Fig. 8b) with increasing concentrations of TiO₂, FeO and to a minor extent MnO and MgO. Assuming stoichiometry, calculated Fe₂O₃ significantly decreases after heating. Because we cannot determine the vacancy concentration from electron microprobe analyses, we calculated formulae assuming stoichiometric composition (three cations, four oxygens) and plotted the data along the stoichiometric tmt series line (grey dot and black square in Fig. 8b). The ulvöspinel component (X_{usp}), calculated from the microprobe data following Stormer (1983), is 0.515 for the unheated and 0.657 for the heated sample (Table 2). Calculating the T_C from this composition and using the regression curves for tmt-ilm_{ss} synthesized at 1100 °C given in Lattard *et al.* (2006), we obtain an average T_C of 236 °C for the unheated and 109 °C for the heated sample. While both, calculated and measured

T_C is in relative good agreement for the heated sample, the T_C calculated for the unheated sample is significantly different. Considering the measured T_C from the κ - T curve (495 °C, Table A2) instead of the calculated T_C (236 °C), the unheated sample shows a high oxidation state of almost $z = 1$ (black dot in Fig. 8b). This observation strongly suggests that during measurement in argon atmosphere, an annealing process occurs, which retransforms the tmgh back into a stoichiometric tmt (or at least into a phase with much less vacancies) because successive heating-cooling κ - T curves are almost perfectly reversible (Fig. 8a).

6.3 Thermal demagnetization of NRM

Thermal demagnetization curves of NRM measured under ambient air conditions all look similar, independent of type deduced from κ - T curves. An example for type 2 and type II of the KH1 drill core is presented in Fig. 9. Type 2 sample reveals an almost constant course of magnetization until about 300 °C. During further heating a continuous decrease occurs until about 500 °C followed by a sudden drop resulting in a blocking temperature below 600 °C. Type II sample shows a continuous decrease until a kink at about 500 °C, which is followed by a blocking temperature at about 550 °C. After each demagnetization step, we measured susceptibility to check if chemical alteration occurred during heating. Susceptibility decrease of type 2 sample is less pronounced than in type II sample, which agrees well with the κ - T curves. The unblocking temperature ranges are extremely broad and many samples have lost 50 per cent of their NRM already at about 300 °C. The fact that some of the observed unblocking temperatures are higher than T_C from κ - T curves might indicate some inversion into a magnetite-near composition during heating. The palaeomagnetic analyses indicate the presence of a stable magnetic component. The inclination-only test provides a mean inclination closer to the expected one (77°) in both cores (in prep.).

7 DISCUSSION

7.1 Comparison between 'young' Krafla and 'old' Stardalur hydrothermally altered basalts

The drill core data of the Krafla geothermal field suggest that the maghemitization of titanomagnetite in this environment not only involves low-temperature oxidation but also mineral reactions, which

Table 2. (a) Electron microprobe data of titanomaghemite in wt. per cent and formulae calculated for three cations and four oxygen for unheated and heated sample KH1–85.25 (type II); n is number of analyses. We analysed six grains in each sample. (b) Calculation of ulvöspinel component in titanomaghemite (X_{Usp}) and Curie temperature (T_c) before (unheated) and after (heated) κ - T measurement.

(a)	Unheated		Heated	
	Mean	(SD)	Mean	(SD)
n	24		21	
SiO ₂	0.19	0.09	0.29	0.16
TiO ₂	16.79	0.52	21.59	1.58
Al ₂ O ₃	1.61	0.32	1.57	0.15
Cr ₂ O ₃	0.05	0.02	0.07	0.03
Fe ₂ O ₃	31.85	1.08	23.22	3.47
FeO	42.72	0.42	47.12	2.07
MnO	2.95	0.19	3.26	0.97
MgO	0.03	0.03	0.12	0.14
CaO	0.23	0.08	0.26	0.06
Na ₂ O	0.01	0.02	0.02	0.02
K ₂ O	0.01	0.01	0.01	0.01
Total	96.44	0.58	97.53	0.76
Si	0.01	0.004	0.01	0.006
Ti	0.49	0.016	0.62	0.046
Al	0.07	0.014	0.07	0.007
Cr	0.00	0.001	0.00	0.001
Fe ³⁺	0.93	0.030	0.67	0.098
Fe ²⁺	1.39	0.014	1.50	0.069
Mn	0.10	0.006	0.11	0.031
Mg	0.00	0.002	0.01	0.008
Ca	0.01	0.003	0.01	0.002
Na	0.00	0.001	0.00	0.002
K	0.00	0.001	0.00	0.001
Total	3		3	

(b)	Unheated		Heated	
	Mean	(SD)	Mean	(SD)
(1) X_{Usp}	0.515	0.016	0.657	0.056
(2) $T_{c\text{cal}}$	236	13.6	109	52.5
(3) $T_{c\text{meas}}$	495	-	110-220	-
(4) X_{Usp}	0.195	-	0.657-0.534	-

Notes:

- (1) X_{Usp} calculated from formula in (a) according to Stormer (1983).
- (2) T_c calculated from X_{Usp} in (1) using formula given in Lattard *et al.* (2006).
- (3) T_c s retrieved from κ - T curves.
- (4) X_{Usp} calculated with T_c from (3) using formula given in Lattard *et al.* (2006).

All temperatures are in °C. *SD*, standard deviation.

cause a significant change of NRM and magnetic susceptibility values. Compared to hydrothermally altered basalts of the distinctly older Staldalur volcano in Iceland (*ca.* 1.8 Ma), which is distinguished by extremely high NRM (18–121 A m⁻¹) and susceptibility values (47–118 × 10⁻³ SI), the Krafla samples show similar maximum susceptibility (0.2–140 × 10⁻³ SI) but NRM values rarely higher than 5 A m⁻¹. The altered basalts from the Krafla drill cores show low NRM, not only compared to the anomalous high NRM values of the Staldalur volcano but also compared to surface basalts of Iceland younger than about 11.5 ka (Fig. 2).

Both, the Staldalur and Krafla basalts have a similar tholeiitic melt composition (Fridleifsson & Kristjansson 1972; Nicholson & Latin 1992). In both areas the basalts are hydrothermally metamorphosed in the chlorite zone and show similar Fe-Ti oxide minerals and textures [compare fig. 4 in Vahle *et al.* (2007) with Fig. 4 of

this study). A significant difference in magnetomineralogy of both localities is the occurrence of symplectic magnetite after olivine, secondary magnetite and magnetite as alteration product of iron sulphides in Staldalur basalts (Vahle *et al.* 2007), which has not been observed in Krafla basalts. Furthermore, the Staldalur basalts show T_V s suggesting a maximum vacancy concentration of 0.003 (Aragón *et al.* 1985), which is significantly lower than in the Krafla samples with a high oxidation state (about $z = 1$). The cation-deficient and Ti-free magnetite observed in κ - T curves of the Staldalur basalts (reversible when measured in argon atmosphere but irreversible in air) is interpreted to be the carrier of the strong remanent magnetization (Vahle *et al.* 2007).

From our observations of the Krafla samples the lower susceptibility in the cooling run of κ - T curves and its stability during repeated heating indicate an inversion of the titanomaghemite during heating into a stable titanomagnetite with higher X_{Usp} component and lower susceptibility. We suggest that either titanium from the neighbouring sphene diffuses back to the titanium-poor tmgh or the tmgh loses Fe³⁺ (microprobe data suggest that Ti/Fe ratio increases after heating). This inversion is different to what we observed for cation-deficient mt from Staldalur [annealing towards stoichiometric mt during heating in argon atmosphere; Vahle *et al.* (2007)]. The Krafla samples indicate additionally to an annealing of vacancies with heating, a diffusion of titanium, probably from the intimate intergrowth with sphene, back into the spinel lattice to produce a stable tmt composition after the heating experiment in an argon atmosphere (Figs 7b and 8a). No T_V occurs after the heating experiment confirming that composition of a mt-near phase has been significantly modified. Our observations indicate a strong mobility of Ti. This difference in behaviour between the Krafla and the Staldalur samples, both hydrothermally overprinted, can be explained by the fact that in Krafla a geothermal system is still active producing significantly metastable tmgh, while in the 1.8-Myr old Staldalur samples the geothermal system is extinct. Therefore the Staldalur samples probably had time to recover and form more stable, near-stoichiometric mt with only a small degree of cation deficiency.

7.2 High magnetic susceptibility and its low field dependence

High magnetic susceptibility is always related to a large quantity of magnetic minerals and it strongly depends on the Ti/(Ti + Fe) ratio and oxygen fugacity of the melt (e.g. Gee & Kent 1997; Brachfeld & Hammer 2006; Vahle *et al.* 2007;). The Icelandic basalts are Fe-richer and more oxidized in their magma composition than Mid-ocean-ridge-basalts (MORB; e.g. Meyer *et al.* 1985). Therefore the ferrimagnetic mineral content at Krafla is significantly higher than in marine environments, where basalts tend to have less than 5 vol. per cent of tmt, and correspondingly, lower susceptibility values (Shau *et al.* 2004). The ferrimagnetic mineral content at Krafla is comparable to the one from Staldalur (Vahle *et al.* 2007), and from surface samples at Reykjanes. The large variation of susceptibility values from 0.2 up to 140 × 10⁻³ SI in the Krafla drill cores with respect to the surface samples at Krafla and Reykjanes (less than 51 × 10⁻³ SI, unpublished own results and Dietze *et al.* 2011), gave rise to the hypothesis that maghemitization causes such high values; and low values are related to hydrothermal mineral reactions that destroy the magnetic minerals.

When the oxidation degree in synthetic titanomaghemite is higher than 0.5–0.6, maghemitization is reported to increase susceptibility values due to a decrease in magnetostriction (Özdemir &

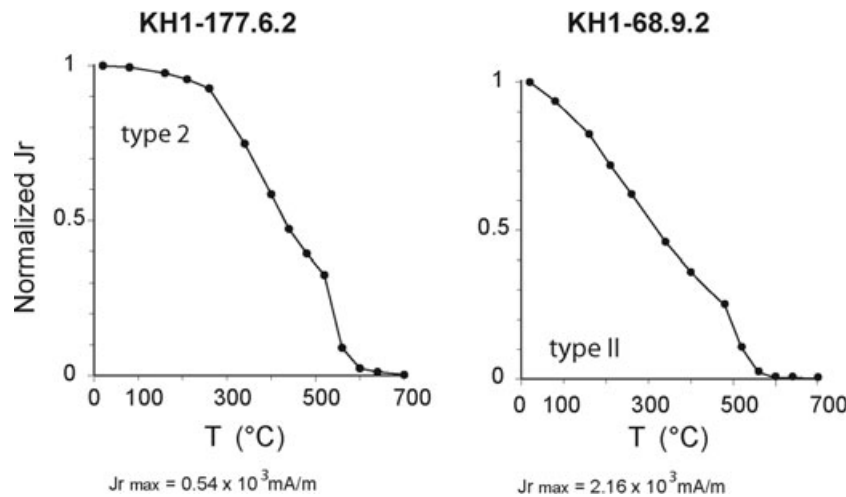


Figure 9. Decay of the natural remanent magnetization (J_r) during thermal demagnetization for type 2 and II curves.

O'Reilly 1982). According to Peters & Dekkers (2003) magnetic susceptibility of mgh ($632 \times 10^{-6} \text{ m}^3 \text{ kg}^{-1}$) is larger than for tmt ($422 \times 10^{-6} \text{ m}^3 \text{ kg}^{-1}$) but lower than for mt ($674 \times 10^{-6} \text{ m}^3 \text{ kg}^{-1}$). These data suggest that there could be, at maximum, a factor of about 1.5 for a susceptibility enhancement if tmt is transformed to mgh. These considerations lead us to suppose that there must be another explanation for the enhanced susceptibility, which remains unclear. However, the key may lie in the microstructure observed by TEM (compare e.g. Xu *et al.* 1997; Zhou *et al.* 2001). In the inlay of Fig. 6(a) maghemite shows a nanoporous microstructure, which has been observed in all investigated grains from the Krafla drill cores (two samples, about 10 different places) but not in other samples (see Fig. 6b). Similar nanoporous maghemites are however described for Chinese palaeosols. It is proposed that microbes in soil environment produce locally reducing environment causing an *in situ* precipitation of nanocrystals, although nanoporous maghemites are also observed as oxidation product of magnetites (Chen *et al.* 2005). These authors suggest such kind of maghemite bio-product as the source of superparamagnetic particles and as the main mechanism of magnetic susceptibility enhancement. Although we did not find any other evidence for superparamagnetic behaviour (e.g. frequency dependence of magnetic susceptibility at room temperature), the nanoporous textures in our samples resemble those of the described new precipitated nanocrystals in soils.

It is interesting to note the low field dependency of magnetic susceptibility of the Krafla samples. Usually, tmt with intermediate Ti concentration show field dependence (see Table A1 for definition of f_{Hd}) up to about 35 per cent (e.g. de Wall 2000; Vahle & Kontny 2005). The maghemitized basalts of the Krafla drill cores show a very low f_{Hd} (less than 3 per cent) even for samples with significant Ti concentrations like KH1-85.25 (Tables 2 and A1). Therefore, low-temperature oxidation seems to affect the field dependence of susceptibility significantly. A possible explanation might be a decrease of the magnetocrystalline anisotropy as the highly anisotropic Fe^{2+} diffuses out of the lattice (O'Reilly 1983). It is known that field dependence of magnetic susceptibility is higher in larger grains due to the rearrangement of domain walls and microstructures (e.g. Hrouda *et al.* 2006). The decrease of the magnetocrystalline anisotropy combined with the influence of grain size reduction due to the observed different processes, might explain the low field dependence of magnetic susceptibility in the maghemitized Krafla samples.

7.3 Low NRM

The fresh and young surface basalts (<11.5 ka) from Reykjanes and Krafla area have NRM values in average of about 20 A m^{-1} while the hydrothermally altered basalts from the Krafla drill cores (<500 ka) mostly show NRM values in average below 3 A m^{-1} .

With distance to the mid-ocean ridge axis, a strong decrease of NRM and magnetic field amplitude to about 20 per cent of the original values have been documented (e.g. Bleil & Petersen 1983), and most NRM values reported for MORB older than 15 Ma are below 3 A m^{-1} (Bleil & Petersen 1983; Wang *et al.* 2005). This value is similar to the mean value of 4 A m^{-1} reported by Kristjansson & Jonsson (2007) for Tertiary lava (1–15 Ma) sampled in Iceland. However, these authors also report values between 0.1 and about 20 A m^{-1} due to the inhomogeneous magnetization of the lava. For the East Pacific Rise axis, Gee & Kent (1994) estimated a rapid magnetization decrease of young MORB from 55 to 10 A m^{-1} within a decay time of about 20 ka. These decay rates of NRM are similar to the one we observe for the Icelandic basalts.

Acidic and corrosive hydrothermal fluids in up-flow zones within the oceanic crust are known to alter or replace the iron-rich magnetic minerals and reduce the NRM, in some cases to zero (e.g. Ade-Hall *et al.* 1971). Reduced crustal magnetization beneath active and extinct hydrothermal vent fields is, for example, described for the TAG (Trans-Atlantic Geotraverse) hydrothermal field on the Mid-Atlantic Ridge (Tivey *et al.* 1993) and the Juan de Fuca Ridge hydrothermal vent field (Tivey & Johnson 2002), and causes local magnetic anomaly lows within the oceanic crust. Geophysical surveys in continents also reveal hydrothermal alteration processes to be a major controlling factor for magnetite destruction accompanied by a decrease of magnetic intensity (Airo 2002). All these observations are similar to those in Iceland, where local magnetic anomaly lows are related to active high-temperature geothermal areas like on Reykjanes and within the Krafla caldera. Apart from primary differences in lava flows (quantity, type of ferromagnetic minerals), there is certainly a decay of NRM related to geothermal alteration in the Krafla area.

A cycling of iron from titanomagnetite to iron sulphide by anaerobe sulphate reducing bacteria has been described by Carlut *et al.* (2007) as a possible mechanism for a significant remanence loss of oceanic basalts. The discrimination of biologically produced minerals from inorganic precipitations is however difficult. In the Krafla samples there are textures and variation of temperatures registered

in the boreholes that may suggest the existence of bio-forming minerals. One texture is the nanoporous maghemite mentioned earlier, and the other texture is the presence of pyrite within the netlike structure of the tmgh and not only around the former tmgh grain (Fig. 5d). This texture forms part of the type III κ - T curves that in turn represent the altered end-member with the dissolution of tmgh and the precipitation of pyrite as secondary mineral. This alteration produces samples with very low susceptibility and NRM values (Fig. 3 and Tables 1 and A1). In addition, the borehole temperature of KH1 in the year 1991 changed from about 85–120 °C at around 80 m to about 150 °C at 175 m depth. Borehole temperature of KH3, measured in 2002, show about 30 °C at about 320 m (Jónsson *et al.* 2003). Therefore, strong variations in temperature with time seem to occur in the geothermal field, which facilitates the contribution of bacteria to bio-formed minerals. Mid-ocean ridge axes are favourable environments for life and important amounts of cells are reported in water close to hydrothermal vents (e.g. Carlut *et al.* 2007).

7.4 Mobility of cations

The mineral reactions given in Section 5.3 imply diffusion under wet conditions not only of Fe^{2+} but also of Ti^{4+} , probably at different rates, out of the tmt lattice, producing tmgh with different Ti content. A diffusion of Ti out of the spinel structure can be explained by the mobility of Ti from tmt with high to intermediate X_{Usp} as $\text{Ti}(\text{OH})_4$ species at low pH conditions (Stefánsson 2001). Dissolution experiments from Stefánsson *et al.* (2001) suggest dissolution of ilmenite above 200 °C and of ulvöspinel up to 300 °C, while pure magnetite is stable at all temperatures. The strong irreversibility of most of the κ - T curves and thermal demagnetization implies that pure magnetite is only a minor phase in our samples and that the NRM is mainly carried by tmgh.

200–300 °C is exactly the temperature interval at which the observed hydrothermal minerals chlorite, chlorite–smectite and pyrite are reported to be stable in the Krafla geothermal system (e.g. Gudmundsson & Arnórsson 2005). The intimate intergrowth of tmgh with sphene and cation-deficient mt (mgh), as it is shown in Fig. 4(d), can be easily explained by the interrelation between oxidation and mineral reaction. The diffusion of Fe^{2+} to the surface of the crystal is well demonstrated in Fig. 5(b), where tmgh with sutured grain boundaries is surrounded by chlorite, suggesting that Fe^{2+} , released from the oxide has reacted to form chlorite. These mineral reactions cause an increase of porosity (Fig. 6a) promoting a better fluid–rock interaction.

The age of geothermal systems and the internal structure of rocks, which controls the surfaces between the fluid and the rock are significant factors controlling the intensity of hydrothermal alteration (Stefánsson *et al.* 2001). Maghemite, especially Ti-rich one, is metastable and will react even more easily with hydrothermal fluids, especially in an acidic environment with enhanced porosity (see eq. 7, and Worm & Banerjee 1984). After the latest Krafla eruptions in 1984, an increase in H_2S and H_2 has been reported by Arnórsson (1995), which acidified the hydrothermal fluids. In addition, the precipitation of pyrite (see eq. 6 and Fig. 5d) is an indication of further acidification of the environment. While ilmenite has already been transformed to sphene or rutile, which is stable under these conditions, tmgh will be dissolved (see Figs 5c and d) resulting in a major loss of magnetic susceptibility and a further decay of remanent magnetization due to the decreasing quantity of magnetic minerals.

8 CONCLUSIONS

Multiple processes related to the geodynamic setting, the emplacement, cooling history (oxygen fugacity), and also the hydrothermal alterations are able to affect the texture and composition of originally homogeneous titanomagnetite (see e.g. fig. 11 in Vahle *et al.* 2007). Basalts from the active geothermal field at Krafla, NE-Iceland are altered in the chlorite zone due to fluid–rock interactions causing maghemitization (low-temperature oxidation) and other mineral reactions. Concerning the magnetic minerals, a two-stage transformation mechanism is suggested.

(1) Dissolution of Ti at low pH under oxidizing conditions from titanomagnetite (ulvöspinel component) and ilmenite to form rutile or sphene and Fe^{2+} migration out of the spinel lattice forming titanomaghemite.

(2) Formation of pyrite and dissolution of remaining titanomaghemite under reducing and acidic conditions.

These two processes are responsible for the significant decrease of NRM intensity (all from 106 investigated samples except in six that have $\text{NRM} > 5 \text{ A m}^{-1}$). However, the observed high susceptibility values (up to $4.9 \times 10^{-5} \text{ m}^3 \text{ kg}^{-1}$), compared to the fresh surface samples cannot be explained satisfactory. In Stardalur, similar high magnetic susceptibility is related to neocrystallization of magnetite from fluids (Vahle *et al.* 2007). However, no indication of such mechanism is seen in Krafla (and NRM values are much lower than in Stardalur samples). A suggested mechanism for the enhancement of the magnetic susceptibility values is related to the observed nanoporous microstructure of the titanomaghemite. This microstructure may induce a superparamagnetic-like behaviour (high susceptibility and low remanence) and it would also explain the low remanence values. In addition to the previously suggested mineral and fluid–rock interactions it also explains local magnetic anomaly lows within the oceanic crust and volcanic islands like Iceland or Hawaii related to hydrothermal alteration. A possible relationship between nanoporous microstructures and microbial activities is a speculation, which needs further investigations.

ACKNOWLEDGMENTS

The funding to carry out this project comes from DFG grant number: KO 1514/3. V. Zibat, M. Fotouhi and R. Schneider are acknowledged for their support in the laboratory for electron microscopy and microprobe analyses at the Karlsruhe Institute of Technology (KIT). The University of Michigan is thanked for the use of the X-ray diffractometer. We appreciate the comments from Rob van der Voo on this manuscript. Ralf Engelmann is acknowledged for discussions about the microprobe results and Manuel Grimm and Sebastian Most for rock magnetic properties measurements on surface basalts from the Krafla area. We are grateful to Leo Kristjánsson for his collaboration. We also want to thank Omar Friedleifson, Asgrímur Gudmundsson, Anett Blischke and Bjarni Gautason from Iceland Geosurvey, for their support on getting access to the drill core samples. We would like to thank E. Petrovsky and an anonymous reviewer for their constructive comments on this manuscript. The editor E. Appel is also acknowledged for the helpful handling of the manuscript.

REFERENCES

- Ade-Hall, J.M., Palmer, H.C. & Hubbard, T.P., 1971. The magnetic and opaque petrological response of basalts to regional hydrothermal alteration, *Geophys. J. R. astr. Soc.*, **24**(2), 137–174.

- Airo, M.L., 2002. Aeromagnetic and aeroradiometric response to hydrothermal alteration, *Surv. Geophys.*, **23**, 273–302.
- Aragón, R., Buttrey, D.J., Sheperd, J.P. & Honig, J.M., 1985. Influence of nonstoichiometry on the Verwey transition, *Phys. Rev.*, **B31**, 430–436.
- Ármansson, H., Benjaminsson, J. & Jeffrey, A.W.A., 1989. Gas changes in the Krafla geothermal system, Iceland, *Chem. Geol.*, **76**, 175–196.
- Arnórsson, S., 1995. Geothermal systems in Iceland: structure and conceptual models-I. High temperature areas, *Geothermics*, **24**(5–6), 561–602.
- Banerjee, S.K., 1971. Decay of marine magnetic anomalies by ferrous ion diffusion, *Nature Phys. Sci. (Lond.)*, **229**(6), 181–183.
- Bitter, F., 1931. On inhomogeneities in the magnetization of ferromagnetic materials, *Phys. Rev.*, **38**, 1903–1905, doi:10.1103/PhysRev.38.1903.
- Bleil U. & Petersen, N., 1983. Variations in magnetization intensity and low temperature titanomagnetite oxidation of ocean floor basalts, *Nature*, **301**, 384–387.
- Bödvarsson, G.S., Benson, S.M., Sigurdsson, Ó., Stefánsson, V. & Elíasson, E.T., 1984. The Krafla geothermal field, Iceland 1. Analyses of well test data, *Water Resour. Res.*, **20**, 1515–1530.
- Brachfeld, S.A., & Hammer, J., 2006. Rock-magnetic and remanence properties of synthetic Fe-rich basalts: implications for Mars crustal anomalies, *Earth planet. Sci. Letters*, **248**, 599–617.
- Brown, A.P., & O'Reilly, W., 1999. The magnetism and microstructure of pulverized titanomagnetite, Fe_{2.4}Ti_{0.6}O₄: the effect of annealing, maghemitization and inversion, *Phys. Earth planet. Int.*, **116**(1–4), 19–30.
- Carlut, J., Horena, H. & Janotsa D., 2007. Impact of micro-organisms activity on the natural remanent magnetization of the young oceanic crust, *Earth planet. Sci. Lett.*, **253**(3–4), 497–506.
- Chen, T., Xu, H., Xie, Q., Chen, J., Ji, J. & Lu H., 2005. Characteristics and genesis of maghemite in Chinese loess and paleosols: mechanism for magnetic susceptibility enhancement in paleosols, *Earth planet. Sci. Lett.*, **240**, 790–802.
- Cui, Y., Verosub, K.L. & Roberts A., 1994. The effect of low-temperature oxidation on large multi-domain magnetite, *Geophys. Res. Lett.*, **21**(9), 757–760.
- Deng, C., Zhu, R., Jackson, M.J., Verosub, K.L. & Singer, M.J., 2001. Variability of the temperature-dependent susceptibility of the Holocene eolian deposits in the Chinese loess plateau: a pedogenesis indicator, *Phys. Chem. Earth*, **26**(11–12), 873–878.
- Dietze, F., Kontny, A., Heyde, I. & Vahle C., 2011. Magnetic anomalies and rock magnetism of basalts from Reykjanes (SW-Iceland), *Stud. Geophys. Geodaet.*, **55**(1), i–xxii.
- Fridleifsson, I.B. & Kristjánsson, L., 1972. The Stardalur magnetic anomaly, *Jökull*, **22**, 69–78.
- Gaillot, Ph., Saint-Blanquant, M. & Bouchez, J.L., 2006. Effects of magnetic interactions in anisotropy of magnetic susceptibility: models, experiments and implications for igneous rock fabric quantification, *Tectonophysics*, **418**, 3–19.
- Gee J. & Kent D.V., 1994. Variations in layer 2A thickness and the origin of the central anomaly magnetic high, *Geophys. Res. Lett.*, **21**, 297–300.
- Gee, J. & Kent D.V., 1997. Magnetization of axial lavas from the southern East Pacific Rise (14 degrees -23 degrees S); geochemical controls on magnetic properties, *J. geophys. Res., B, Solid Earth and Planets* **102**, 24 873–24 886.
- Gee, J., Schneider, D.A. & Kent, D.V., 1996. Marine magnetic anomalies as recorders of geomagnetic intensity variations, *Earth planet. Sci. Lett.*, **144**(3–4), 327–335.
- Gíslason, S.R. & Arnórsson S., 1993. Dissolution of primary basaltic minerals in natural waters: saturation state and kinetics, *Chem. Geol.*, **105**, 117–135.
- Gudmundsson, Á., 1993. Cross section between wells BJ-11 and BJ-12 in Bjarnarflag, National Energy Authority Report OS-93071/JHD-35 B, 46 pp (in Icelandic).
- Gudmundsson, B.T. & Arnórsson S., 2002. Geochemical monitoring of the Krafla and Námafjall geothermal areas, N-Iceland. *Geothermics*, **31**, 195–243.
- Gudmundsson, B.T. & Arnórsson S., 2005. Secondary mineral: fluid equilibria in the Krafla and Námafjall geothermal systems, Iceland. *Appl. Geochem.*, **20**(9), 1607–1625.
- Gudmundsson, G., Pálmason, G., Grönvold, K., Ragnars, K., Saemundsson, K. & Arnórsson, S., 1971. Námafjall – Krafla: progress report on the investigation of the geothermal areas, N.E.A. Geothermal division, p. 81.
- Haggerty, S.E., 1991. Oxide textures: a mini-atlas, in *Oxide Minerals: Petrologic and Magnetic Significance*, Vol. 25, pp. 129–219, ed. Lindsley, D.H., Mineralogical Society of America, (Reviews in Mineralogy) Chantilly, VA, USA.
- Hall, J.M., 1985. The Iceland Research Drilling Project crustal section: variation of magnetic properties with depth in Icelandic-type oceanic crust, *Canadian J. Earth Sci.*, **22**(1), 85–101.
- Hrouda, F., Clupáková, M. & Mrázová S., 2006. Low-field variation of magnetic susceptibility as a tool for magnetic mineralogy of rocks, *Phys. Earth planet. Inter.*, **154**, 323–336.
- Irving, E., 1970. The Mid-Atlantic ridge at 45 degrees N.: XIV. Oxidation and magnetic properties of basalt: review and discussion, *Canadian J. Earth Sci.*, **7**(6), 1528–1538.
- Jackson, M., Moskowitz, B., Rosenbaum, J., Kissel, C., 1998. Field-dependence of AC susceptibility in titanomagnetites, *Earth planet. Sci. Lett.*, **157**, 129–139.
- John, C.M., 2004. Plotting and analyzing data trends in ternary diagrams made easy, *EOS, Trans. Am. geophys. Un.*, **85**(16), 158. http://www.agu.org/eos_elec/000562e.shtml.
- Jónsson, S.S., Gudmundsson, A. & Thordarson S., 2003. Krafla. Borun kjarnaholu KH-3 milli Jörundar og Háganga. Íslenskar orkurannsóknir, ÍSOR-2003/015. Unnid fyrir Landsvirkjun.
- Juárez, M.T., Tauxe, L., Gee, J.S. & Pick T., 1998. The intensity of the Earth's magnetic field over the past 160 million years, *Nature*, **304**, 878–881.
- Just, J., 2005. Modification of magnetic properties in granite during hydrothermal alteration (EPS-1 borehole, Upper Rhine Graben), *PhD thesis*. University of Heidelberg.
- Kadko, D., Gronvold, K. & Butterfield, D., 2007. Application of radium isotopes to determine crustal times of hydrothermal fluids from two sites of Reykjanes Peninsula, Iceland, *Geochim. Cosmochim. Acta*, **71**, 6019–6029.
- Kent, D.V. & Gee, J., 1994. Grain size-dependent alteration and the magnetization of ocean basalts, *Science*, **265**, 1561–1563.
- Kletetschka, G. & Kontny, A., 2005. Identification of magnetic minerals by scanning electron microscope and application of ferrofluid, in *The Castle Meeting*, Studia Geophysica et Geodetica, Vol. **49**(2), pp. 153–162, ed. Petrovsky, E., Springer, Dordrecht.
- Kontny A., Vahle, C. & de Wall H., 2003. Characteristic magnetic behaviour of subaerial and submarine lava units from the Hawaiian Scientific Drilling Project (HSDP-2), *Geochem. Geophys. Geosyst.*, **4**(1), doi:10.1029/2002GC000304.
- Krása, D. & Herrero-Bervera E., 2005. Alteration induced changes of magnetic fabric as exemplified by dykes of the Koolau volcanic range, *Earth planet. Sci. Lett.*, **240**, 445–453.
- Kristjánsson, L. & Jonsson, G., 2007. Paleomagnetism and magnetic anomalies in Iceland, *J. Geodyn.*, **43**, 30–54.
- Lattard, D., Engelmann, R., Kontny, A. & Suerzapf, U., 2006. Curie temperatures of synthetic titanomagnetites in the Fe-Ti-O system: effects of composition, crystal chemistry, and thermomagnetic methods, *J. geophys. Res.*, **111**, B12S28, doi: 10.1029/2006JB004591.
- Marshall, M. & Cox, A., 1972. Magnetic changes in Pillow Basalt due to sea floor weathering, *J. geophys. Res.*, **77**(32), 6459–6469.
- Meyer, P.S., Sigurdsson, H. & Schilling, J-G., 1985. Petrological and geochemical variations along iceland's neovolcanic zones, *J. geophys. Res.*, **90**(B12), 10 043–10 072.
- Moore, D.M. & Reynolds R.C., 1997. *X-Ray Diffraction and the Identification and Analysis of Clay Minerals*, Oxford University Press, New York, NY, 378pp.
- Nicholson, H. & Latin D., 1992. Olivine tholeiites from Krafla, Iceland: Evidence for variations in melt fraction within a plume, *J. Petrol.*, **33**(5), 1105–1124.
- O'Reilly, W., 1983. The identification of titanomagnetites: model mechanisms for the maghemitization and inversion process and their magnetic consequences. *Phys. Earth planet. Inter.*, **31**: 65–76.

- Özdemir Ö., 1987. Inversion of titanomaghemites. *Phys. Earth planet. Inter.*, **46**, 184–196.
- Özdemir, Ö. & O'Reilly, W., 1982. Magnetic hysteresis properties of synthetic monodomain titanomaghemite, *Earth planet. Sci. Lett.*, **25**, 406–418.
- Peters, C. & Dekkers, M.J., 2003. Selected room temperature magnetic parameters as a function of mineralogy, concentration and grain size, *Phys. Chem. Earth*, **28**(16–19), 659–667.
- Petersen, N. & Vali, H., 1987. Observation of shrinkage cracks in ocean floor titanomagnetite, *Phys. Earth planet. Inter.*, **46**, 197–205.
- Petrovsky, E. & Kapicka, A., 2006. On determination of the Curie point from thermomagnetic curves, *J. geophys. Res.*, **111**, B12S27, doi: 10.1029/2006JB004507.
- Poulton, S.W., Krom, M.D. & Raiswell R., 2004. A revised scheme for reactivity of iron (oxyhydr)oxide minerals towards dissolved sulfide, *Geochim. Cosmochim. Acta*, **68**, 3703–3715.
- Prérot, M., Remond, G. & Caye R., 1968. Etude de la transformation d'une titanomagnetite en titanomaghemite dans une roche volcanique, *Bull. Soc. Fr. Mineral. Cristallogr.*, **91**, 65–74.
- Pyzik, A.J. & Sommer S.E., 1981. Sedimentary iron monosulphides: kinetics and mechanism of formation, *Geochim. Cosmochim. Acta*, **45**, 687–698.
- Readman, P.W. & O'Reilly W., 1972. Magnetic properties of oxidized (cation-deficient) titanomagnetites (Fe, Ti)₃O₄, *J. Geomagn. Geoelectr.*, **24**, 69–90.
- Saemundsson, K., 1978. Fissure swarms and central volcanoes of the neovolcanic zones of Iceland, *Geol. J.*, **10**, 415–432.
- Saemundsson, K., 1991. Geology of the Krafla system, in *The Natural History of Lake Myvatn*, pp. 24–95, eds. Gardarsson, A. & Einarsson, P. (in Icelandic), The Icelandic Natural History Society, Reykjavik.
- Saemundsson, K. & Pringle M., 2003. Evolution of the Krafla Central volcano, north volcanic zone, Iceland, *EOS, Trans. Am. geophys. Un.*, **84**(46), Fall Meet. Suppl., Abstract V32D-1052.
- Shau, Y.H., Torii, M., Horng, C.S. & Liang, W.T., 2004. Magnetic properties of mid-oceanic-ridge-basalts from Ocean Drilling Program LEG 187, in *Proceedings of the Ocean Drilling Program, Scientific Results*, Vol. **187**, pp. 1–25, eds. Pedersen, R.B., Christie, D.M. & Miller, D.J., IODP Publications, College Station, TX.
- Smith, B., 1987. Consequences of the maghemitization on the magnetic properties of submarine basalts: synthesis of previous works and results concerning basement rocks from mainly D.S.D.P. Legs 51 and 52, *Phys. Earth planet. Inter.*, **46**, 206–226.
- Stefánsón, A., 2001. Dissolution of primary minerals of basalt in natural waters I, calculation of mineral solubilities from 0 °C to 350 °C, *Chem. Geol.*, **172**, 225–250.
- Stefánsón, A. & S. Arnórsson, 2002. Gas pressures and redox reactions in geothermal fluids in Iceland, *Chem. Geol.*, **190**, 251–271.
- Stefánsón, A., Gíslason, S.R. & Arnórsson, S., 2001. Dissolution of primary minerals in natural waters II, mineral saturation state, *Chem. Geol.*, **172**, 251–276.
- Steinthórsson, S. & Sveinbjörnsdóttir A.E., 1981. Opaque minerals in geothermal well N° 7, Krafla, northern Iceland, *J. Volc. Geotherm. Res.*, **10**, 245–261.
- Stormer, J. C., Jr., 1983. The effects of recalculation on estimates of temperature and oxygen fugacity from analyses of multicomponent iron-titanium oxides, *Am. Mineral.*, **68**, 286–294.
- Tivey, M.A. & Johnson H.P., 2002. Crustal magnetization reveals subsurface structure of Juan de Fuca Ridge hydrothermal vent fields, *Geology (Boulder)*, **30**(11), 979–982.
- Tivey, M.A., Rona, P.A. & Schouten H., 1993. Reduced crustal magnetization beneath the active sulfide mound, TAG hydrothermal field, Mid-Atlantic Ridge at 26°N, *Earth planet. Sci. Lett.*, **115**, 101–115.
- Vahle C. & Kontny, A., 2005. The use of field dependence of AC susceptibility for the interpretation of magnetic mineralogy and magnetic fabrics in the HSDP-2 basalts, Hawaii, *Earth planet. Sci. Lett.*, **238**, 110–129.
- Vahle C., Kontny, A., Gunnlaugsson, H.P. & Kristjánsson. L., 2007. The Stardalur magnetic anomaly revisited: new insights into a complex cooling and alteration history, *Phys. Earth planet. Inter.*, **164**, 119–141.
- Vogt, P.R. & Johnson, G.L., 1973. Magnetic telechemistry of oceanic crust?, *Nature*, **245**, 373–375.
- de Wall, H., 2000. The field-dependence of AC susceptibility in titanomagnetites: implications for the anisotropy of magnetic susceptibility, *Geophys. Res. Lett.*, **27**, 2409–2411.
- Wang, D. & Van Der Voo, R., 2004. The hysteresis properties of multidomain magnetite and titanomagnetite/ titanomaghemite in mid-ocean ridge basalts, *Earth planet. Sci. Lett.*, **220**(1–2), 175–184.
- Wang, D., Van Der Voo, R. & Peacor, D.R., 2005. Why is the remanent magnetic intensity of Cretaceous MORB so much higher than that of the mid to late Cenozoic MORB?, *Geosphere*, **1**(3), 138–146.
- Wang, D., Van Der Voo, R. & Peacor, D.R., 2006. Low-temperature alteration and magnetic changes of variably altered pillow basalts. *Geophys. J. Int.*, **164**(1), 25–35.
- White, A.T., Peterson, M.L. & Hochella, M.F., 1994. Electrochemistry and dissolution kinetics of magnetite and ilmenite, *Geochim. Cosmochim. Acta*, **58**(8), 1859–1875.
- Worm, H.U. & Banerjee, S.K., 1984. Aqueous low-temperature oxidation of titanomagnetite, *Geophys. Res. Lett.*, **11**(3), 167–172.
- Xu, W., Peacor, D.R., Dollase, W.A., Van Der Voo, R. & Beaubouef, R., 1997. Transformation of titanomagnetite to titanomaghemite: a slow, two-step, oxidation-ordering process in MORB, *Am. Mineral.*, **82**, 1101–1110.
- Zhou, W., Van Der Voo, R., Peacor D.R. & Mansfield, J.F., 1999. Determination of lattice parameter, oxidation state, and composition of individual titanomagnetite/ titanomaghemite grains by transmission electron microscopy, *J. geophys. Res.*, **104**(8), 17 689–17 702.
- Zhou, W., Peacor, D.R., Alt, J.C., Van Der Voo, R. & Kao, L.S., 2001. TEM study of the alteration of interstitial glass in MORB by inorganic processes, *Chem. Geol.*, **174**(1–3), 365–376.

APPENDIX

Table A1. Rock magnetic properties for standard specimen of a volume of 10 cm³. κ_{300} is magnetic susceptibility measured in a field of 300 A m⁻¹. Mass susceptibility is magnetic susceptibility normalized by mass (χ). f_{Hd} (per cent) is field dependence of magnetic susceptibility. NRM is natural remanent magnetization. Q is Königsberger ratio [for calculation of f_{Hd} (per cent) and Q see footnote below the table). MDF is median destructive field determined from AF demagnetization curves of NRM.

Sample	Depth (m)	Lithology	κ_{300} (10 ⁻³ SI)	Mass susceptibility (10 ⁻⁵ m ³ kg ⁻¹)	f_{Hd} (per cent)	NRM (A m ⁻¹)	Q	MDF (mT)
KH1 68.90 1	68.95	Fine grained basalt	139.00	4.877	0.7194	1.894	0.3	23
KH1 69.4 1	69.40	Fine grained basalt	100.00	3.937	0.5000	3.862	0.9	4
KH1 69.4 2	69.40	Fine grained basalt	96.10	3.100	0.9365	4.199	1.1	–
KH1 80.50 1	80.30	Vesicular basalt	23.50	0.887	0.0000	0.8059	0.8	–
KH1 80.50 2	80.30	Vesicular basalt	9.54	0.409	0.4193	1.764	4.5	–
KH1 83.20 1	83.40	Vesicular basalt	0.24	1.26E – 02	–1.2500	0.01025	1.0	–
KH1 83.20 2	83.40	Vesicular basalt	0.31	1.47E – 02	0.3205	0.02165	1.7	18
KH1 85.25 1	85.25	Vesicular basalt	117.00	4.134	1.7094	0.9031	0.2	9
KH1 85.25 2	85.25	Vesicular basalt	66.30	2.393	1.3575	1.52	0.6	–
KH1 85.75 2	85.75	Vesicular basalt	0.85	3.20E – 02	0.0000	0.1067	3.0	33
KH1 174.5 1	174.55	Tuff with b layers	3.50	0.139	0.0000	0.9087	6.2	–
KH1 174.5 2	174.55	Tuff with b layers	3.35	0.129	0.0000	0.9309	6.7	–
KH1 174.7 1	174.75	Tuff with b layers	0.38	1.60E – 02	0.0000	0.01415	0.9	29
KH1 177.6 1	177.60	Tuff with b layers	9.27	0.316	0.2157	0.5752	1.5	20
KH1 179.70 1	179.70	Basalt intrusion	23.10	0.819	1.7316	0.6742	0.7	–
KH1 179.70 2	179.70	Basalt intrusion	54.90	1.981	2.1858	1.245	0.6	–
KH1 180.00 1	180.00	Basalt intrusion	9.01	0.371	0.9989	0.3316	0.9	–
KH1 180.00 2	180.00	Basalt intrusion	30.00	1.282	1.0000	1.132	0.9	–
KH1 187.4 1	187.40	Basalt	58.40	1.959	2.5685	1.624	0.7	–
KH-1 187.4 2	187.40	Basalt	67.20	2.301	2.2321	3.093	1.1	–
KH3 36.0 1	36.00	Basalt	24.00	0.767	1.2500	2.656	2.7	–
KH3 36.0 2	36.00	Basalt	23.20	0.748	1.2931	2.995	3.1	–
KH3 38.8 1	38.80	Basalt	24.10	0.820	1.2448	3.094	3.1	–
KH3 38.8 2	38.80	Basalt	22.90	0.771	0.8734	2.808	3.0	–
KH3 41.2 1	41.20	Basalt	37.00	1.117	2.9730	1.583	1.1	–
KH3 41.2 2	41.20	Basalt	33.20	1.074	2.7108	1.722	1.3	–
KH3 46.7 1	46.70	Basalt	23.20	0.814	0.8621	3.349	3.5	–
KH3 46.7 2	46.70	Basalt	21.10	0.708	0.4739	3.633	4.2	22
KH3 49.3 2	49.35	Basalt	41.70	1.345	1.9185	2.21	1.3	–
KH3 58.0 1	58.00	Basaltic breccia	7.03	0.253	–0.7112	1.916	6.5	8
KH3 58.0 2	58.00	Basaltic breccia	7.41	0.274	0.1350	1.595	5.2	–
KH3 188.5 1	188.50	Basalt	0.76	3.27E – 02	0.0000	0.03295	1.0	–
KH3 188.5 2	188.50	Basalt	0.83	3.60E – 02	0.3628	0.03702	1.1	–
KH3 190.05 1	190.00	Basalt	21.40	0.836	0.4673	2.413	2.7	–
KH3 190.05 2	190.00	Basalt	6.43	0.255	0.0000	0.7857	2.9	–
KH3 195.1 1	195.05	Basalt	79.60	3.302	0.7538	4.812	1.5	–
KH3 195.1 2	195.05	Basalt	36.50	1.705	0.2740	3.648	2.4	–
KH3 199.05 1	199.00	Porphyritic basalt	32.00	1.311	0.3125	2.654	2.0	–
KH3 199.05 2	199.00	Porphyritic basalt	19.70	0.821	0.0000	2.124	2.6	–
KH3 199.70 1	199.65	Porphyritic basalt	41.00	1.774	0.2439	3.76	2.2	–
KH3 199.70 2	199.65	Porphyritic basalt	49.80	2.083	0.2008	4.636	2.2	–
KH3 289.7	289.65	Pillow basalt	2.67	0.114	0.3745	0.7323	6.6	–
KH3 289.8	289.8	Pillow basalt	30.00	1.149	0.3333	4.122	3.3	–
KH3 292.35 1	292.35	Basalt	78.20	2.984	0.5115	12.43	3.8	–
KH3 292.35 2	292.35	Basalt	70.70	2.688	0.2829	5.919	2.0	–
KH3 293.20 1	293.25	Basalt	47.50	1.819	0.0000	3.352	1.7	–
KH3 293.20 2	293.25	Basalt	51.70	1.921	0.1934	4.013	1.9	–
KH3 293.85 1	293.85	Basalt	57.00	2.192	0.0000	5.497	2.3	–
KH3 293.85 2	293.85	Basalt	60.40	2.262	0.0000	15.17	6.0	–
KH3 298.4 1	312.35	Basalt	26.10	1.087	0.3831	3.11	2.9	–
KH3 298.4 2	312.35	Basalt	28.50	1.212	0.3509	2.64	2.2	–
KH3 301.90 1	312.55	Contact	43.70	1.791	0.4577	1.86	1.0	–
KH3 301.90 2	312.55	Contact	57.10	2.187	0.8757	2.23	0.9	–
KH3 309.15 1	319.55	Basalt	9.58	0.371	0.4175	1.53	3.8	–
KH3 309.15 2	319.55	Basalt	3.18	0.131	0.0000	1.21	9.1	–
KH3 312.3 1	370.50	Basaltic andesite	45.20	1.779	0.4425	4.72	2.5	–

Table A1. (Continued)

Sample	Depth (m)	Lithology	κ_{300} (10^{-3} SI)	Mass susceptibility (10^{-5} m ³ kg ⁻¹)	f_{Hd} (per cent)	NRM ($A\ m^{-1}$)	Q	MDF (mT)
KH3 312.3 2	370.50	Basaltic andesite	44.30	1.751	0.2257	4.23	2.3	–
KH3 312.57 1	371.20	Basaltic andesite	40.60	1.573	0.4926	6.36	3.8	–
KH3 312.57 2	371.20	Basaltic andesite	36.10	1.303	0.2770	14.50	9.7	–
KH3 312.75 1	371.60	Basalt	30.90	1.103	0.3236	2.05	1.6	–
KH3 312.75 2	371.60	Basalt	34.10	1.253	0.5865	2.08	1.5	–
KH3 319.5 1	375.40	Basalt	7.67	0.272	0.2608	0.88	2.8	–
KH3 319.5 2	380.40	Basalt	40.20	1.376	0.4975	2.99	1.8	–
KH3 322.4 1	380.40	Basalt	0.54	2.59E – 02	–0.3724	0.00018	0.0	–
KH3 322.4 2	380.50	Basalt	0.45	2.17E – 02	1.1161	0.00041	0.0	–
KH3 370.5 1	380.50	Basalt	30.10	1.063	0.3322	2.12	1.7	–
KH3 370.5 2	389.80	Basalt	34.70	1.261	0.5764	2.03	1.4	–
KH3 371.25 1	394.00	Basalt	13.30	0.448	0.7519	2.79	5.1	–
KH3 371.25 2	394.00	Basalt	15.00	0.503	0.6667	2.77	4.5	–
KH3 371.65 1	395.30	Basalt	24.00	0.848	0.8333	1.37	1.4	–
KH3 371.65 2	395.30	Basalt	29.40	1.038	1.0204	1.52	1.3	–
KH3 373.32 1	373.30	Pillow	7.71	0.317	0.1297	11.00	34.3	–
KH3 373.32 2	373.30	Pillow	19.80	0.742	0.5051	19.40	23.7	25
KH3 374.05 1	374.00	Pillow	35.00	1.282	0.2857	2.81	1.9	–
KH3 374.05 2	374.00	Pillow	39.30	1.408	0.2545	2.73	1.7	20
KH3 375.45	375.40	Basalt	11.50	0.530	0.0000	9.79	20.4	–
KH3 380.40 1	380.40	Basalt	67.90	2.460	0.5891	1.08	0.4	–
KH3 380.40 2	380.40	Basalt	74.60	2.608	0.5362	2.14	0.7	14
KH3 380.50 1	380.50	Basalt	48.60	1.767	0.2058	2.43	1.2	–
KH3 380.50 2	380.50	Basalt	39.90	1.445	0.2506	2.68	1.6	27
KH3 382.35 1	382.30	Basalt breccia	0.88	–	–1.2346	–	4.3	–
KH-3 382.35 2	382.30	Basalt breccia	0.66	–	0.8197	–	6.4	–
KH3 382.90 1	382.90	Pillow basalt	3.86	0.148	0.2591	1.50	15.6	–
KH3 382.90 2	382.90	Pillow basalt	32.40	1.136	0.3086	1.96	1.7	–
KH3 383.75 1	383.70	Pillow basalt	14.10	0.490	0.0000	0.28	2.6	–
KH3 383.75 2	383.70	Pillow basalt	27.80	0.952	0.3597	0.21	1.7	–
KH3 389.80	389.80	Basalt	49.50	1.903	3.0303	0.13	0.1	–
KH3 391.70 1	391.70	Pillow basalt	3.74	0.133	1.3369	0.51	1.4	–
KH3 391.70 2	391.70	Pillow basalt	2.18	7.60E – 02	0.9174	0.73	1.4	–
KH3 392.05 1	392.05	Pillow basalt	13.10	0.455	1.5267	3.60	1.0	–
KH3 392.05 2	392.05	Pillow basalt	22.80	0.786	0.8772	3.02	0.8	–
KH3 394.00 1	394.00	Basalt	50.70	1.884	0.3945	3.56	1.7	–
KH3 394.00 2	394.00	Basalt	48.60	1.827	0.2058	3.24	1.5	–
KH3 395.30 1	395.30	Basalt	24.00	0.848	0.0000	2.06	3.6	–
KH3 395.30 2	395.30	Basalt	22.10	0.801	0.0000	2.35	3.5	–
KH3 397.60 1	397.60	Pillow basalt	55.10	1.974	0.1815	–	0.9	–
KH3 397.60 2	397.60	Pillow basalt	54.70	1.967	0.1828	–	1.0	–

Note: $f_{Hd}(\%) = (\kappa_{300} - \kappa_{30}) \times 100 / \kappa_{300}$ $Q = NRM / \kappa \times 41.63 \times 10^{-3} (A\ m^{-1})$.

Table A2. Verwey transition (T_V) or isotropic point (T_i). Curie (T_C) temperatures and transition temperatures (T_t) retrieved from $1/\kappa$ - T and κ - T curves for KH1 and KH3 drill cores using Petrovsky & Kapicka (2006) and Lattard *et al.* (2006) methods, respectively). (h) Heating. (c) Cooling run T_{t1} , T_{t2} , T_{t3} are transition temperatures during one heating or cooling run. T_{V2} and T_{V3} are Verwey transitions measured after a first or second heating-cooling cycle. NP, not present; ND, not done; All temperatures are in °C. In Grey: transition points from the κ - T curves.

A.T.2.1. First run in Argon atmosphere										
Sample	Depth (m)	Lithology	T_V/T_i	T_t (h)	T_C (h)	T_C (c)	T_t (c)	T_{V2}		
KH1 68.90 1	68.95	Fine grained basalt	-144	483	534	533	263	NP		
KH1 69.4 2	69.40	Fine grained basalt	decay at -85	491	571	571	432	NP		
KH1 80.5	80.30	Vesicular basalt	NP	-	566	566	-	NP		
KH1 83.20 2	83.40	Vesicular basalt	NP	-	451	500	267	NP		
KH1 85.25 1	85.25	Vesicular basalt	decay at -144	495	543	560	195	NP		
KH1 85.75 2	85.75	Vesicular basalt	NP	-	562	566	269	NP		
KH1 174.5	174.55	Tuff with basalt layers	-151	-	580	584	-	ND		
KH1 174.7 1	174.75	Tuff with basalt layers	NP	-	580	584	-	-136		
KH1 177.6 1	177.60	Tuff with basalt layers	-157	320	568	558	250	-156		
KH1 179.70 1	179.70	Intrusion	NP	500	573	485	320	NP		
KH1 180.00 2	180.00	Intrusion	-161	507	575	580	-	NP		
KH1 187.4 1	187.40	Basalt	-152	511	582	580	-	NP		

Sample	Depth (m)	Lithology	T_V/T_i	T_{t1} (h)	T_{t2} (h)	T_{t3} (h)	T_C (h)	T_C (c)	T_{t1} (c)	T_{t2} (c)	T_{V2}
KH3 36.0 1	36.00	Basalt	-161	-	-	480	580	537	-	-	NP
KH3 46.7 2	46.70	Basalt	-148	-	-	-	587	588	317	-	ND
KH3 49.3 2	49.35	Basalt	-153	-	-	496	580	577	474	-	NP
KH3 198.65	198.50	Porphyritic basalt	-155	138	340	570	582	578	556	265	NP
KH3 199.05 2	199.00	Porphyritic basalt	-157	146	337	570	593	581	554	-	NP
KH3 199.70 2	199.65	Porphyritic basalt	-147	142	316	574	633	588	562	-	-143
KH3 292.35 1	292.35	Basalt	-149	148	329	477	577	576	562	268	-161
KH3 293.20 1	293.25	Basalt	NP	-	-	142	585	576	394	-	ND
KH3 293.85 2	293.85	Basalt	-145	-	145	335	580	583	393	-	NP
KH3 298.4 1	298.4	Pillow basalt	-146	142	341	508	587	591	325	-	-167
KH3 301.90 2	301.95	Pillow basalt	-150	141	365	531	607	604	573	356	-173
KH3 309.15 2	309.1	Pillow basalt	NP	142	512	-	585	594	572	406	ND
KH3-3 312.3.1	312.35	Basalt	-144	140	380	-	567	560	394	-	ND
KH3 312.57 2	312.55	Contact	NP	141	329	483	576	560	332	-	ND
KH3 312.75 1	312.75	Pillow basalt	-155	140	402	-	561	574	554	329	-141
KH3 322.4 2	322.40	Andesite	NP	-	-	568	585	582	320	-	-142
KH3 373.32 2	373.30	Pillow	NP	141	-	-	568	556	-	-	ND
KH3 374.05 2	374.00	Pillow	-153	147	384	-	570	580	409	-	ND
KH3 380.40 2	380.40	Basalt	-163	300	-	564	583	581	545	297	decay
KH3 380.50 2	380.50	Basalt	-161	143	380	-	570	563	379	-	NP
KH3 394.0 1	394.00	Basalt	-161	-	362	545	568	593	547	360	NP
KH3 395.30 1	395.30	Basalt	-144	145	324	480	571	564	350	-	ND

A.T.2.2. Second run in Argon atmosphere						
Sample	T_t (h)	T_C (h)	T_C (c)	T_t (c)	T_{V3}	
KH1 68.90 1	-	560	558	260	NP	
KH1 69.4 2	463	570	568	441	ND	
KH1 83.20 2	312	584	587	-	-142	
KH1 85.25 1	100	566	536	100	NP	
KH1 174.7 1	-	580	577	348	Decay -120	

Sample	T_{t1} (h)	T_{t2} (h)	T_C (h)	T_C (c)	T_{t1} (c)	T_{t2} (c)	T_{V3}
KH3 292.35 1	-	-	630	626	330	-	-167
KH3 322.4 2	-	580	606	588	470	240	-145
KH3 380.40 2	-	295	576	581	295	-	Decay at -175